UNIVERSITAT POLITÈCNICA DE CATALUNYA
BARCELONATECH
Escola Superior d'Enginyeries Industrial,
Aeroespacial i Audiovisual de Terrassa

BACHELOR FINAL THESIS

Study of an UAV implementation for solar panel cleaning

Document:

Report

Author:

Miriam Martínez Ambrosio

Director/Co-director:

Fatiha Nejjari Akhi-elarab

Degree:

Bachelor's degree in Aerospace Technology Engineering

Examination session:

Spring 2023

Acknowledgements

This study could not have been developed without the guidance and support of the thesis director, Fatiha Nejjari Akhi-elarab. A very special thank you to her for being my advisor, for all the time devoted to this project, and for her continuous encouragement.

The author extends also her gratitude to her family and friends, whose unconditional love and encouragement have eased not only the process of this thesis but also in her academic career. A special shout out to my dad, without whom the proposed implementation would not have come to my mind.

Abstract

The upcoming rise in solar panels is a reality. The EU has already elaborated a specific strategy for solar energy in the project *REPowerEU*, which is intended to boost renewable sources. Since one of solar energy's main complexities is their efficiency drop when dirt or dust is accumulated in the panels, this thesis comes up with a new proposal for cleaning them: using an UAV. After a study of all the possible methods for cleaning solar panels, some drones used for this task were found. However, their duty tends not to be enough for being the only method employed.

With the aim of proposing an innovative solution, specific payloads for performing the task will be added to an already-in-the-market drone. Therefore, the best cleaning methods and UAVs are examined. After analyzing several models, *Matrice 300 RTK* from *DJI* is selected as the most suitable one through the *OWA* method. Moreover, a robotic manipulator and a mop coated with microfiber cloth are selected as the payload to carry out the cleaning since a previous study demonstrated its effectiveness. The payload's dimensions and general characteristics are designed according to the UAV's features.

Then, the prototype mathematical model is computed considering the manipulator and the drone as two distinct bodies whose forces affect one another. Having computed the mathematical model, simulations are conducted using *MATLAB/SIMULINK* so as to validate it. Furthermore, two control schemes are implemented for ensuring stability in the system; a *PID* for the manipulator and a *LQG regulator* for the quadrotor. The control was only developed for the hover condition, which corresponds to when the manipulator performs its task. Finally, after reviewing the prototype's environmental impact and economic feasibility, some considerations and future proposals are made.

Keywords: UAV, robotic manipulator, UAV equipped with a robotic arm, solar panel cleaning, Matrice 300 RTK, quadrotor mathematical modeling, control, LQG regulator, PID.

Abstracte

L'imminent augment de panells solars és una realitat. La UE ja ha desenvolupat una estrategia específica per a l'impuls de l'energia solar en el projecte *REPowerEU*, que té l'objectiu de fomentar l'ús de les energies renovables. Donada la disminució d'eficiència dels panells quan s'acumula brutícia o pols, aquesta tesi planteja una nova proposta per a la neteja d'aquests: l'ús d'un UAV. Després d'un estudi de tots els mètodes existents per a la neteja de panells solars, es van trobar alguns drons ja destinats a aquesta feina. Tanmateix, la seva aplicació acostuma a necessitar d'un altre mètode per a aconseguir la neteja desitjada.

Amb l'objectiu de proposar una solució innovadora, s'afegirà una càrrega específica dissenyada per la neteja a un dron ja existent en el mercat. Per aquest motiu, s'analitzen els millors mètodes que es podrien utilitzar i els UAV que hi ha. D'aquest anàlisis i mitjançant un *OWA* el model *Matrice 300 RTK* de l'empresa *DJI* és el seleccionat. A més a més, s'estableix que un braç robòtic i una mopa recoberta d'un drap de microfibres conformaran la càrrega destinada per a la neteja. Aquesta selecció està basada en els resultats obtinguts en un estudi experimental. Les dimensions i característiques principals de la càrrega son dissenyats amb les consideracions pertinents de l'UAV.

Tot seguit, es calcula el model matemàtic del prototip considerant el braç i el dron com a dos cossos independents que interaccionen mitjançant les forçes. Un cop es determina aquest, es realitzen simulacions utilitzant el software *MATLAB/SIMULINK* per a la validació. A més a més, s'implementen dos esquemes de control per tal de garantitzar l'estabilitat del sistema; un *PID* pel braç i un regulador *LQG* pel que fa el quadrotor. El control es desenvolupa només per a la condició de vol estacionari, ja que en aquesta és on el braç actuarà. Finalment, després d'analitzar els possibles impactes tant ambientals com econòmics del prototip, es realitzen algunes consideracions i propostes futures.

Paraules clau: UAV, braç robòtic, UAV equipat amb un braç robòtic, neteja de plaques solars, Matrice 300 RTK, model matemàtic d'un quadrotor, control, regulador LQG, PID.

Contents

List of Figures

List of Tables

List of abbreviations / Glossary

UAV Unmanned Aerial Vehicle

VTOL Vertical Takeoff and Landing

MALE Medium-altitude long endurance

HALE High-altitude long endurance

UAS Unmanned Aircraft System

MTOW Maximum Takeoff Weight

VLOS Visual line of sight

BCS Brush cleaning system

ECS Electrostatic cleaning system

HCS Heliotex cleaning system

RCS Robotic cleaning system

CCS Coating cleaning system

PV Photovoltaic

UV Ultraviolet

LQR Linear Quadratic Regulator

LQG Linear Quadratic Gaussian

RTK Real Time Kinematic

EU European Union

OWA Ordered weighted average

SHOP Super Hydrophobic Plane

SHIP Super Hydrophilic Plane

DC Direct Current

GPS Global Positioning System

GNSS Global Navigation Satellite System

IMU Inertial Measurement Unit

IEC International Electrotechnical Comission

ESC Electronic Speed Controller

AMC Acceptable Means of Compliance

GM Guide Material

EASA European Union Aviation Safety Agency

STS Standard Scenarios

PID Proportional-integrative-derivative

Chapter 1

Introduction

1.1 Object

The aim of this project is to study the implementation and development of an UAV capable of performing the cleaning tasks of solar panels.

1.2 Scope

The contents that will be included in this final project are the following:

- Analysis of the existing cleaning methods for solar panels, so as to choose the most suitable one.
- Determination of the payload needed for the final cleaning method.
- Selection of the most appropriate existing UAVs for this task.
- Study of the mathematical control model, including the equations, the controllers, and the control system design appropriate for this kind of system.
- Simulation of the control system using *MATLAB/SIMULINK*.
- Definition of the prototype that will be used and its 3D model.
- Study of the proposed prototype's economic and technical feasibility.
- Study of the environmental impact this implementation could have.
- EU regulations for civil drones will be taken into account.

On the other hand, some tasks will be left out of the scope:

- A brand-new UAV will not be designed since the proper payload will be added to an already existing one.
- The specific materials required for the prototype will not be detailed.

- The real implementation of the proposed solution will not be included in this study.

The following deliveries will be handed in:

- Project charter: This is the first document to develop. It includes a brief description of what the study consists of and how everything is intended to be managed.
- Report: The report is the most important document as it will contain all the student work.
- Budget: This document will include the costs of the study's realization.
- Blueprints: As the present study includes a 3D modelling of the UAV, its drawings will be provided too.

1.3 Requirements

The UAV will be designed considering the following requirements:

1. The system should be able to clean roofs' solar panels.
2. Panels located 10 m below should be cleanable.
3. The UAV should be capable of hovering for, at least, 30 minutes.
4. The simulation will be implemented using *MATLAB/SIMULINK*.
5. The 3D prototype will be done using *SOLIDWORKS*

1.4 Rationale

Since May 2022, Europe has established a plan to cut off its dependency on Russia's fossil fuels and to help avoid climate change: **REPowerEU**. Therefore, an increase in renewable sources is expected, in which Solar Energy is included. Being the latter the one source of energy with the highest growing pace, there is a specific strategy for it. The idea is to boost the rooftops' potential to produce energy by implementing photovoltaics in all kinds of buildings: public, commercial, and residential[1].

The expected rise in solar cells would lead to an increase on the jobs related to solar energy. The more panels to install, the more trained personal is required for whether installing or reparing them [2]. Not only would new jobs be generated but bills could also be reduced. In fact, a system that connects various flats to a rooftop full of panels in Odet Court in Cardiff, Wales, has reduced the residents' bill by half [3]. Having such an impact in society's economy, Europe's solar energy proposal is likely to success.

Once the upcoming increase in photovoltaics has been mentioned, their proper maintenance should be born in mind. Keeping solar panels cleaned is a key to preserve their effectiveness as well as for increasing their lifetime. Up to an 85% of effectiveness in performance can be lost due to dust accumulation [4]. As technology evolves, several cleaning methods have been developed in order to ease their maintenance. One of the newest solutions consists in using UAVs for cleaning solar panels.

Nowadays, there exist UAVs capable of doing all the cleaning and UAVs in charge of carrying a special washing robot. Since most of the former have not been fully implemented yet, this brand-new solution has still room for improvement. Companies such as *SolarDrone* [5] and *Cleandrone* [6] will shortly place their drones in the market. Nevertheless, their aim is to clean panels in esplanades. Another similar example is *Drone Volt*'s UAVs [7], for instance, which are already working and capable of cleaning roofs (not solar cells in roofs). The latters require human interaction and the water is supplied using a pump connected to the UAV.

The companies previously mentioned as well as others will be considered with a view to design the most suitable UAV for solar panels' maintenance.

Chapter 2

State of the art

Fossil fuels have been the primary source of energy since the Industrial Revolution. Nevertheless, not only their depletion but also the pollution produced when converting these sources into energy have encouraged the European Union to shift towards renewable energy sources [8]. Ambitious targets have been set, such as the **REPowerEU** plan which intends to achieve the 45% of the energy consumed in the EU to come from renewable sources [9]. In fact, in 2021 the percentage reached was 22%.

The projects developed for achieving the desired percentage are based particularly on wind and solar power [8]. The latter is actually the fastest-growing renewable energy. Therefore, the possibility of it being tripled by 2026 is also born in mind as the following graphic portrays [9].

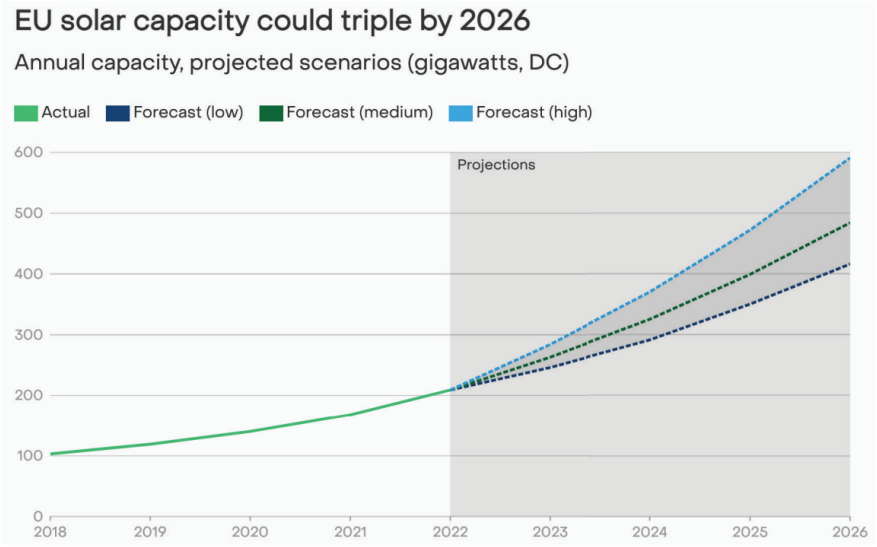

Figure 2.1: Solar power growth and projected scenarios (*Source: [10]*).

This increase is expected considering the solar energy strategy in *REPowerEU*, which consists on three different initiatives [1]:

- Implementing photovoltaics on the rooftops so as to produce energy

- Promoting the development of skilled professionals in the sector
- Creating a commission to ensure the objectives are met

However, the implementation of photovoltaics is pointless unless the panels are properly maintained. This has been demonstrated in several experiments reviewed in the literature. It has been determined that dust accumulated in the panel can lead up to an 85% loss of effectiveness to create energy [4].

2.1 Cleaning methods review

Once the importance of having neat solar panels has been highlighted, the procedure required for obtaining them should be given some thought. There are several ways of cleaning PV cells, from using specialized robots to coating the panels' surface. The most detailed methods in the literature are the ones that will be described hereafter, which can be divided into four main categories [4].

2.1.1 Natural cleaning

The first category consists in taking advantage of the weather for dusting since some agents such as wind, rain, or melting snow are capable of it [4].

The wind is an ideal natural agent for removing large particles. However, dust becomes attached to the panel in high-humidity areas, making the wind insufficient for detaching. [11] Regarding rain, although it is considered the most effective natural agent, sometimes it is not neat enough to wash the cells. Therefore, a layer of mud can be accumulated on the panels, making them even harder to clean [12].

Each natural agent has a list of advantages and disadvantages that their use implies. The following table summarizes the considerations that should be made before deciding on only using weather conditions for cleaning.

Advantages	**Disadvantages**
- It does not need an investment [13]	- Weather is uncontrollable [12]
- Some weather conditions can fully clean the panels [13]	- Only large particles are removed [12]
	- Sometimes it can increase dust depositions [13]
	- The climate is influenced by the location of the panels [12]

Table 2.1: Pros and cons of using natural cleaning

2.1.2 Manual cleaning

The most common technique is manually performing solar cells maintenance. A brush with or without a supply of water, and even sometimes soap, are used for this procedure. Although the brush material is a key factor, skilled professionals are also needed to prevent the panels from being scratched [12, 14, 15].

Finally, one should bear in mind the positive and negative impacts of this method:

Advantages	Disadvantages
- Efficient cleaning [16]	- Expensive [13]
- High efficiency improvement [16]	- Dangerous for the staff [15]
- All the corners can be properly wiped	- Large amounts of water are used [14]
- All kinds of dust particles are removed	- It requires a considerable amount of time [14]
	- Direct contact of the brushes may be abrasive for the panels [12]

Table 2.2: Pros and cons of manually cleaning

2.1.3 Passive surface treatment

The Coating Cleaning System (CCS) is considered a self-cleaning method in which the panels are coated with materials that prevent dust adhesion by making them repellent [16]. Two strategies can be implemented: super-hydrophilic films or super-hydrophobic films. Both of them have a limited lifetime, which makes re-coating after a certain time a must. Hence, the performance of the solar collectors could worsen as years goes by [13].

Super Hydrophobic Plane (SHOP)

This method uses materials with water-repellent properties, such as silicones, silanes, nanoparticles, and polymers, to coat the surface. Efficiency depends on the used material [16]. The coating material forms a thin layer that prevents water from sticking to the surface of the cell [17]. Then, as water moves along the panel, it washes the dirt. Therefore, SHOP is ineffective in dry climates [12].

Super Hydrophilic Plane (SHIP)

It consists in a nano-film made of TiO_2 with similar properties to the materials used in SHOP coating. The main difference is that SHIP is able of decomposing dirt and dissolving it in water using ultraviolet light. The coating behaves as a suspension material for dust [17]. Although it is more enduring than SHOP, UV rays end up deteriorating the coating. It is not a useful method for dry areas since regular washings would then be required since, once again, water is a must for removing dirt [12].

Some positive and negative factors of these procedures should be contemplated and, hence, are attached below:

Advantages	Disadvantages
- Although water is needed, there is less water consumption [16]	- Dust clusters could be formed [16]
- It does not require power supply [16]	- Materials may be expensive [16]
- Can last for a couple of years [13]	- Lifetime is limited [13]
	- Not useful for dry climates [12]

Table 2.3: Pros and cons of passive surface treatment

2.1.4 Automated cleaning system

This last category embraces a wide variety of procedures for soiling mitigation. What all of them have in common is their capability of accomplishing automatically the task using controlled mechanical devices [13].

Electrostatic Cleaning System (ECS)

The ECS requires the solar panels to have mounted electrodes parallel to the surface. Once the dust is accumulated, it can be lifted away due to the charges differences originated by stimulating dirt with a high alternating current [16]. It only ensures the removal of dry dust and the electrodes activate when the weight on the panels surpasses a certain value. The process is automated using a microcontroller [14].

The pros and cons of implementing ECS are the following:

Advantages	**Disadvantages**
- Takes short time for removing dust [16]	- The electric field generated has high intensisty [16]
- Low energy and power consumption [16]	- Not useful for all kind of particles, an external method is needed [16]
- No mechanical friction, thus, no surface damage [16]	- It is still in development [13]
- No water usage [16]	- Expensive [12]
	- UV rays can degradate the screen [12]

Table 2.4: Pros and cons of ECS

Water Cleaning Systems

In this case, large quantities of high-pressure water are used for washing solar cells. This is considered an improved solution of the rainfall method since it can be programmed and controlled. Moreover, cleansing agents can be added so as to perfect the result [12]. The water is conducted through pumps and pipes, and this method also helps in cooling the panels' temperature [17].

There is a developed system named *Heliotex Cleaning System (HCS)*, in which nozzles located in the corners of the panels are used for ejecting the water. For controlling the system and knowing when can it work or when to stop a sensor is used [16]. Moreover, liquid soap is added for improving performance. Not only do the nozzles require monitorization, but also the soap level [15].

Figure 2.2: Heliotex cleaning method. *Source: Solar panel cleaning systems*

As the previous methods, employing only water for cleaning has its benefits and weaknesses too. These have been collected in the table below:

Advantages	**Disadvantages**
- Improved rainfall cleaning [12]	- Loss of a large amount of water [12]
- It cools the panels what enhances efficiency [12]	- Thermal shock could happen [12]
	- More dust is attracted after the clean [12]
	- Tanks need to be manually refilled [16]
	- Sticky particles are not removed [16]
	- Pipes have the risk of being blocked or broken [17]
	- Maintenance of nozzles and soap levels are required [15]

Table 2.5: Pros and cons of water cleaning

Mechanized Cleaning

As its name states, in this method, mechanical devices such as engines or robots, are used. A combination of sensors and a precise controlling system determine when is it necessary to begin the procedure. In this process, as the system moves above the panels, having lightweight mechanisms is essential [12].

There are two types of Mechanized Cleaning: Brush Cleaning System (BCS), and Robot Cleaning System (RCS). The former consists in a moving brush or wiper powered by an external DC motor. The brush moves around the solar panel cleaning the dirt without water, hence, the brush should be frequently changed. The possibility of scratching the solar collector has to be born in mind as well as the fact that corners cannot be reached [16]. The difference with the RCS is that while BCS only uses brushes, RCS can use other cleaning tools such as wipers or pads, or even an air blower [14]. Nevertheless, the combination of BCS and RCS is what tends to be used.

Eccopia E4 is an example of a robot composed of a photovoltaic panel, a battery, and microfiber brushes capable of dry cleaning, without water. It moves along the panels through a fixed rail. On the other hand,

there are other prototypes that work with water, which perform a wet cleaning, such as *Washpanel*. Moreover, this robot moves vertically and cleans horizontally trying to enhance the results [15].

In [12] a brand-new robot implementation that combines autonomous brushes with electrostatic precipitators has been proposed. The latter is used for collecting the accumulated dust particles in the brush. The robot starts the procedure only when the accumulated dust layer is thicker than what was specified by the user. Furthermore, time is reduced by placing the brushes in the longitudinal direction to the panels.

Figure 2.3: Automated robotic brush (*Source:[12]*).

Another simpler prototype is designed in [18]. This model uses an Arduino microprocessor and considers a parking station in which the robot can be charged. The brush is driven by a DC motor and the whole system uses rails to get from one side to the other of the panel. It should be highlighted that this example is just to demonstrate the efficiency of this cleaning method even with a not-so-highly-complex prototype.

The considerations that should be made before implementing a Mechanized Cleaning System are pointed out below.

Advantages	**Disadvantages**
- Independent and automatic systems [12]	- Brushes in direct contact with the panels can be abrasive [12]
- The installation or the robot can scare birds [12]	- The mechanical parts need maintenance [12]
- Less labour cost [12]	- The weight of the mechanism in the panel cannot be neglected [17]
- Improves cleaning access to the panel as it can operate horizontally or vertically [19]	- More power consumption [17]
- Withstands different climate conditions [19]	- High operations and maintenance costs [13]
- Low on water consumption [16]	

Table 2.6: Pros and cons of Mechanized Cleaning

2.2 UAVs Cleaning Systems

Another Mechanized Cleaning System is the use of UAVs for soiling mitigation in solar panels. Since this is the main objective of the project, more detailed research has been carried out. Firstly, some of the advantages

and disadvantages of using an UAV are considered from the consulted literature and gathered in the table above:

Advantages	Disadvantages
- High mobility of the system [11]	- Short flight time [11]
- Water-free cleaning [11]	- Expensive investment [11]
- It is capable of working completely autonomously [11]	- Requires charging stations [11]
- Its downward thrust can help remove some dust particles [14]	
- The load carried can be a selected cleaning tool [11]	
- Capable of performing continuous operation [19]	
- Pursuing an aerial thermographic inspection is possible[11]	

Table 2.7: Pros and cons of UAVs Cleaning Systems

One of the most remarkable advantages of using UAVs is being able to select the payload carried. Hence, different cleaning methods can be tried out so as to determine which one suits best. In [11], the comparison between implementing a vacuum with a microfiber cloth, a vacuum with a brush, a microfiber cloth on its own, or a brush is made. Although the brush was the easiest to implement in the UAV, the two most effective methods were demonstrated to be microfiber and vacuum and the microfiber wiper itself. However, the mixture of methods not only increases the weight and size of the payload but also the electricity consumption. As a result, it could be concluded that adding a microfiber cloth to an UAV would be the best option.

In addition, the experiment conducted in [11] also studied which was the optimal frequency for cleaning. Weekly cleaning was found to enhance the most efficiency since daily cleaning consumed too much power, and doing it monthly did not have beneficial results.

2.2.1 Proposals

Being a method still in development, there are multiple suggestions that could be developed and improve the performance of the already-in-the-market prototypes. In this section, two approaches will be commented.

The first idea is based on using the downward thrust of an UAV for removing all the dust accumulated. The drone was equipped with a primary camera, a vision pointing system, 3D sensing system, a dual-band GPS, and a high-precision inertial measurement unit so that the surfaces of the solar cells can be properly examined. The UAV used, a quadrotor, was a DJI Inspire 1 drone [14].

The experiment conducted measured the dust after the flight was executed in order to quantify the efficiency of the procedure. Not only was the process studied but also in which pattern was it more effective. The results stated that it was reasonable to begin the cleaning when there was a dust volume of 50 CC and that the best pattern was horizontally moving the UAV [14].

The second proposal is based on trying to implement the *lotus effect*, which alludes to the ability to self-clean and to be water-resistant. The operation process of the method is spraying water at a very high contact angle to achieve the lotus effect. This specific prototype is intended to clean the solar cells located on roofs [20].

The payloads that it would carry are a camera, a GPS sensor, a 3D conical tank, and a transceiver module. The tank could be 3D-printed so as to cheapen the whole prototype. Regarding the transceiver module, it is one in charge of making the transmission of the gathered data possible. For being able of moving that much payload, an hexarotor is needed. Moreover, the UAV will be provided with an intelligent AI framework, using the VGG-16 CNN technique. Therefore, the network should be trained by repeating the whole cleaning process several times. However, some challenges have to be still solved such as the UAV's maximum payload, which affects the amount of water carried, and where could the station be placed [20].

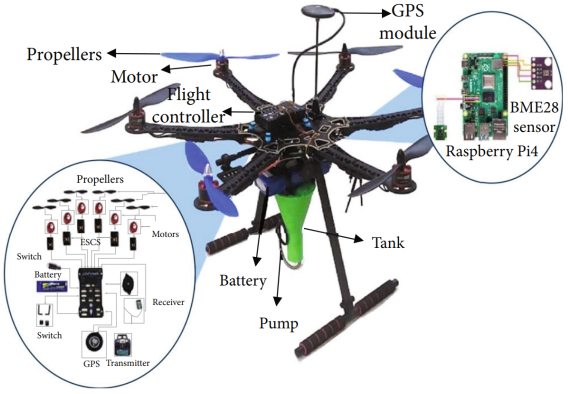

Figure 2.4: UAV designed for implementing the lotus effect (*Source:[20]*).

2.2.2 Already-developed models

On the other hand, there are companies that have already developed and implemented UAVs. Although most of them are intended for solar farm cleaning, the following ones are used on rooftops. *Solarbrush* is an already-developed quadrotor used for cleaning solar panels. It has a tail attached, which is the only part that contacts the panel. The materials of the tail are selected so as to simulate a brush[15]. Another company's UAV, *Cleandrone*, carries a container, in which cleaning liquid is stored and a glass cleaning device [11].

(a) Cleandrone prototype (*Source: [6]*).

(b) Solarbrush prototype. (*Source:[15]*).

Figure 2.5: Examples of already-developed models.

Chapter 3

Methodology

The present study analyzes a new implementation for cleaning solar panels located in rooftops: the use of an UAV. Although some of them have already been developed, there are very few and their benefit compared to other methods is minimum. Furthermore, they tend to be only used on farms. The process of the study will be divided into the following steps:

1. **Prototype general definition:** All the possible UAVs configuration will be compared so as to find the most appropriate one. Moreover, the best cleaning method to apply will also be selected in order to define the necessary payload. With all the previous considerations, the already-developed UAV model will be selected. In this part, the regulations that could be applied for future implementation will be also detailed.

2. **Prototype design:** Since the prototype will be based on an existing UAV, only its payload measures will be computed and its payload components designed. This part will be accomplished using *MATLAB* for the computations and *SOLIDWORKS* for the design.

3. **Modelling of the prototype:** Once all the measures are computed and the UAV is chosen, the mathematical expression that resembles the UAV's behavior will be determined.

4. **Control of the prototype:** Having the model equations developed, the system will be controlled using an LQG as the control technique for the drone. *MATLAB/SIMULINK* will be used for the simulations.

5. **Future impacts:** The proposed solution will be analyzed in terms of environment and economics. This part is essential since the decision regarding the project's continuity depends on it.

This study is only the beginning of a long-term project, which means that all the details of the implementation will not be elaborated. The obtained results could be considered if the prototype's design continues.

Chapter 4

Prototype definition

4.1 General configuration

For selecting the most suitable vehicle, all the possible configurations should be considered. Hence, all types of UAVs are analyzed.

4.1.1 Body architecture classification

Depending on the body architecture of the vehicle there is a general classification[21], in which the most common ones are:

- **Fixed-Wing:** This kind of UAVs have the body shape of a conventional airplane. They need a runway or external help such as a hand or a parachute for taking off and landing. This configuration is advantageous since it allows a larger payload capacity but also a longer flight time.
- **Rotatory-Wing:** They have motors installed in the vehicle's arms so as to produce thrust and propulsion. The motors enable them to take off and land vertically and give them the ability to remain in hover. They resemble helicopters. Nevertheless, their range is shorter as well as their flight time.
- **Vertical Take off and Landing, VTOL:** This last configuration is a mixture of the two previously defined architectures. It has multirotors that enable the vehicle vertically taking off and landing but also a fixed wing for horizontally moving.

In the present project, the UAV that will be used has to be a rotatory-wing, since being capable of hovering is one of the main requirements. Fixed-wing UAVs not only are incapable of hovering but also of maintaining low speeds. Nevertheless, rotatory-wing UAVs are not as ideal as one may believe given that their power consumption is greater than the fixed-wing, hence, they have a lower flight endurance [22].

4.1.2 Range and Weight classification

Another type of organization is by classifying UAVs considering their range and weight as the following table states[22].

Type	Maximum Weight [kg]	Maximum Range [km]	Category
Nano	0.2	5	Fixed wing, rotatory wing
Micro	2	25	Fixed wing, rotatory wing
Mini	20	40	Fixed wing, rotatory wing
Light	50	70	Fixed wing, rotatory wing
Small	150	150	Fixed wing
Tactical	600	150	Fixed wing
MALE	1000	200	Fixed wing
HALE	1000	250	Fixed wing
Heavy	2000	1000	Fixed wing
Super heavy	2500	1500	Fixed wing

Table 4.1: UAV weight and range classification (*Source:[22]*).

The UAV required for cleaning solar panels needs to be able to carry some payload, making *Nano* and *Micro* not an option. As has been previously stated, the body architecture will be a rotatory wing. Therefore, *Mini* and *Light* configurations are acceptable alternatives.

4.1.3 Rotatory-wing UAVs classification

There are various models of rotatory-wing UAVs, which depend on the wings' distribution. The most commonly used are [23]:

- **Single rotor:** This model considers the rotatory-wing UAVs with only one rotor. It is easily maneuverable but has complex mechanics.
- **Axial rotor:** In this case, it is a type of *signle rotor* but the wing is located so that the wind flows parallel to the rotation axis while taking off or landing. Therefore, the mechanics of the *single rotor* get simpler although the aerodynamics become more complicated.
- **Coaxial rotor:** It has two rotatory wings located one on top of the other that rotate reversely. It has simple mechanics but complex aerodynamics.
- **Tandem rotors:** These UAVs have two rotatory wings located each one in one arm of the vehicle, easing the aerodynamics of the *coaxial rotors*. The mechanics are, on their behalf, more complicated.
- **Multirotor:** It follows the same concept as the tandem rotors, there is a rotatory wing in each vehicle's arm. In the most common case, there are four arms (quadrotor) but more elaborated UAVs of six and eight arms exist too. They are named hexacopter and octocopter respectively. However, the more arms are added, the more complex the system gets. The drawback of these models is their high power consumption.

- **Blimp:** This model is an UAV that imitates a blimp. It has complicated maneuverability but does not require much power.
- **Bird-like:** The wings are distributed in order to resemble bird wings leading to complex mechanics. On the other hand, it is easily maneuverable.
- **Insect-like:** This model follows the same design as the *bird-like* but resembling insects.

In order to determine which configuration would be the most suitable for the project, the comparison among these types carried in [23] is considered.

	A	B	C	D	E	F	G	H
Power cost	2	2	2	2	1	4	3	3
Control cost	1	1	4	2	3	3	2	1
Payload/volume	2	2	4	3	3	1	2	1
Maneuverability	4	3	2	2	3	1	3	3
Mechanics simplicity	1	2	3	1	4	4	1	1
Aerodynamics complexity	1	1	1	1	4	3	1	1
Low speed flight	4	3	4	3	4	4	2	2
High speed flight	2	4	1	2	3	1	3	3
Miniaturization	2	3	4	2	3	1	2	4
Survivability	1	3	3	1	1	3	2	3
Stationary flight	4	4	4	4	4	3	1	2
Total	24	28	32	23	33	28	22	24

[1] A=Single rotor, B=Axial rotor, C=Coaxial rotors, D=Tandem rotors, E=Quadrotor, F=Blimp, G=Bird-like, H=Insect-like.

Figure 4.1: Rotatory-wing models comparison (*Source:[23]*).

In the Figure above, each model is given a punctuation from 1 to 4 for specific criteria selected by the author of [23]. When a value of 1 is given it means that the vehicle has poor behaviour in such criteria, thus, a value of 4 corresponds to proper performance. Once all the scores are summed up, *quadrotor* can be concluded to be the best option and, hence, the UAV model that will be used for the prototype.

However, with the aim of ensuring the viability of this proposal, the drones used in the literature should be reviewed. Although more complex multirotors are used for carrying out an extensive cleaning [6, 20], quadrotors are employed for simpler tasks such as carrying a brush [15]. Therefore, the use of a quadrotor is sensible.

4.2 Prototype primarly definition

Before moving on to the selection of the specific configuration of the UAV, the payload that will be carried should be specified, since it is a major aspect to consider in the decision of the UAV model. However, in order to do so, the cleaning method the UAV will implement needs to be decided. From all the reviews carried out in the *State-of-the-art*, section 2.1, four possibilities mentioned in [11] stand out:

1. Implementing a brush.

2. Implementing microfiber cloth.
3. Adding a vacuum to the implementation of a brush.
4. Adding a vacuum to the implementation of a microfiber cloth.

Nevertheless, the research conducted in [11] stated that the most suitable way of cleaning the photovoltaic modules was using a microfiber cloth. Not only was the cleaning more efficient than when the brush was used, but also adding a vacuum only added complexity to the system. Therefore, the idea is to apply a microfiber cloth as payload so as to carry out the cleaning.

In [14] the most effective pattern for the UAV to follow was determined to be moving horizontally. However, as the microfiber cloth was smaller than the solar panel, not all the photovoltaics' surface could be reached. Hence, the microfiber cloth will be attached with one link of a robotic arm that enables the movement of the cloth.

4.2.1 Payload

Once the cleaning method and the payload required are chosen, the weight of each element should be specified. To do so, some commercially available items are taken into account.

Payload	**Weight [kg]**
Robotic arm	0.2
Mop	0.650
Microfiber cloth	0.0294
Total	**0.879**

Table 4.2: Payload initial weights.

The robotic arm's weight is obtained by doing an average of one link's weight in the literature consulted [24, 25, 26, 27]. When it comes to the mop, it has been given a length of 100 cm and has been found in [28]. Lastly, the microfiber cloth's weight is computed taking into account the mop's surface [29].

Since these items may not be the definitive ones, and in order to have a margin in case of error, a total weight of nearly 1 kg is considered.

4.3 Specific configuration

4.3.1 Possible quadrotors

Developing a brand-new UAV is out of the scope, thus, research amongst the available drones in the market is carried out. As has been previously detailed, the UAV employed will be a quadrotor. The first two UAVs selected are from the same brand: Freefly Systems [30].

(a) AltaX. (*Source:[30]*).

(b) Astro. (*Source: [30]*).

Figure 4.2: Freefly Systems' UAVs.

From one of the most known companies, DJI, the models Matrice 300 RTK, Inspire 3, and Phantom 4 V Pro are chosen [31].

(a) Matrice 300 RTK (*Source: [31]*).

(b) Inspire 3 (*Source:[32]*).

(c) Phantom 4 V Pro (*Source: [31]*).

Figure 4.3: DJI's UAVs.

Last, but not least, models Draganflyer Commander 2, ANAFI AI, and Skydio X2e that are respectively from Draganfly [33], Parrot[34], and Skydio [35] are also taken into consideration.

(a) Draganflyer Commander 2 (*Source: [33]*).

(b) Anafi AI (*Source: [34]*).

(c) Skydio (*Source:[36]*).

Figure 4.4: Other brands' UAVs.

The following Table 4.3 contains some information about each UAV's model, such as its maximum payload or whether the vehicle can be retracted.

Model	**Maximum payload [kg]**	**Maximum autonomy [min]**	**Retractable**	**Drawings available**
AltaX	15.9	53	Yes	Yes
Astro	1.5	37	Yes	Yes
Matrice 300 RTK	2.7	55	Yes	Yes
Inspire 3	0.5	25	No	No
Phantom 4 V Pro	-	30	No	No
Draganflyer Commander 2	1	32	Yes	No
ANAFI AI	-	32	Yes	No
Skydio X2E	-	35	Yes	No

Table 4.3: General characteristics of the quadrotors.

However, these parameters are not the criteria used to compare the models. In fact, the characteristics that will be crucial for the vehicle selection are: autonomy, temperature, height and wind resistance. All the available values of such characteristics regarding each model are in the next Table 4.4.

Model	**Autonomy with payload [min]**	**Temparature operation [ºC]**	**Maximum height [m]**	**Wind resistance [m/s]**
AltaX	50	-20 to 50	-	-
Astro	29	-20 to 50	-	10
Matrice 300 RTK	42	-20 to 50	5000-7000	15
Inspire 3	impossible	-20 to 40	3800-7000	12-14
Phantom 4 V Pro	30	0 to 40	6000	10
Draganflyer Commander 2	32	-24 to 38	2438	9
ANAFI AI	32	-10 to 40	5000	12-14
Skydio X2E	35	-10 to 43	3650	10

Table 4.4: Quadrotors' decisive characteristics.

Phantom 4 V Pro, *ANAFI AI*, *Draganflyer Commander 2*, and *Skydio X2E* autonomy depending on the payload is not accessible, so the maximum autonomy is supposed to be the autonomy of the vehicle with the corresponding payload of over 1 kg.

Once the payload's weight has been estimated in section 4.2.1, the maximum autonomy of the vehicle depends on such weight. Moreover, the vital importance of autonomy cannot be neglected as it is one of the project's main requirements. The higher the autonomy, the better, since more photovoltaics could be cleaned. Besides, as the solar panels tend to be located in hot sunny areas, the vehicle should be capable of operating under elevated temperatures. Hence, the higher the maximum operating temperature, the most suitable the UAV. Regarding the height, if the proposed solution wants to be suitable for all kinds of buildings, including skyscrapers, an elevated ceiling is the key. Furthermore, wind gusts are a reality on rooftops, meaning the UAV should be capable of hovering despite their effect. Last but not least, this study could not be conducted

if the drawings of the model are not available, making such feature a decisive criteria too.

Bearing in mind all the characteristics mentioned and their influence, each model is given a score from 1 to 5 for each criteria, the former being the worst performance and the latter the better. It is worth highlighting that the unavailable values and the ones that do not meet the requirements have been given a score of 0.

	Autonomy	**Temperature**	**Ceiling**	**Wind**	**Drawings**
AltaX	5	5	0	0	5
Astro	1	5	0	1.67	5
Matrice 300 RTK	3.46	5	5	5	5
Inspire 3	0	1.62	5	3.67	0
Phantom 4V Pro	1.18	1.62	4.12	1.67	0
Draganflyer Commander	1.56	1	1	1	0
ANAFI AI	1.56	1.62	3.25	3.67	0
Skydio X2E	2.13	2.62	2.06	1.67	0

Table 4.5: Punctuation of the models for each criteria.

The decision-making method employed for identifying the most appropriate quadrotor is named *Ordered Weighted Average (OWA)*. It consists in giving a specific weight to each criteria (g_i), and a grade to each model (p_i), which has already been done in Table 4.5. Then, the *Ordered Weighted Average* is computed following the expression:

$$OWA = \frac{\sum_{i=1}^{n} p_i \times g_i}{p_{max} \times \sum_{i=1}^{n} g_i}$$

Some weights are given to the criteria, being autonomy the most fundamental characteristic, and temperature the least. Tables 4.6, 4.7, and 4.8 show how the OWA result of every model is obtained.

Criteria	**Weight**	**AltaX**		**Astro**		**Matrice 300 RTK**	
	g	**p**	**gxp**	**p**	**gxp**	**p**	**gxp**
Autonomy	15	5	75	1	15	3.46	51.9
Temperature	5	5	25	5	25	5	25
Ceiling	10	0	0	0	0	5	50
Wind	10	0	0	1.67	16.7	5	50
Drawings	10	5	50	5	50	5	50
SUM	50		150		106.7		226.9
OWA			*0.6*		*0.43*		*0.91*

Table 4.6: OWA of the first three models.

Criteria	**Weight**	**Inspire 3**		**Phantom 4V Pro**		**ANAFI AI**	
	g	**p**	**gxp**	**p**	**gxp**	**p**	**gxp**
Autonomy	15	0	0	1.18	17.7	1.56	23.4
Temperature	5	1.62	8.1	1.62	8.1	1.62	8.1
Ceiling	10	4.12	41.2	4.12	41.2	3.25	32.5
Wind	10	1.67	16.7	1.67	16.7	3.67	36.7
Drawings	10	0	0	0	0	0	0
SUM	50		66		83.7		100.7
OWA			*0.26*		*0.33*		*0.4*

Table 4.7: OWA of other three models.

Criteria	**Weight**	**Draganflyer Commander 2**		**Skydio X2E**	
	g	**p**	**gxp**	**p**	**gxp**
Autonomy	15	1.56	23.4	2.13	31.95
Temperature	5	1	5	2.62	13.1
Ceiling	10	1	10	2.06	20.6
Wind	10	1	10	1.67	16.7
Drawings	10	0	0	0	0
SUM	50		48.4		82.35
OWA			*0.19*		*0.33*

Table 4.8: OWA of the rest of models.

Comparing all the possible models, the one with the highest OWA is *Matrice 300 RTK*, from DJI. Furthermore, as Table 4.3 shows, the drawings of such model are available, which eases the prototype design. Therefore, *Matrice 300 RTK* is selected as the UAV used.

4.4 Matrice 300 RTK

Once the UAV has been selected, it will be analyzed in terms of innovative features, components and design parameters.

4.4.1 Features

The selected UAV, the Matrice 300 RTK, has more features than the ones that have been taken into account for the selection process. In this section, the drone will be described and its numerical values will be computed.

Matrice 300 RTK features
- It has a six-directional sensing and positioning system
- Includes safety beacons on top and bottom so as to allow night flights
- The RTK module allows a more accurate positioning
- It has a transmission range of 15 km
- Maximum velocity of 23 m/s
- Wind resistance of 12 m/s
- It can carry multiple payloads (up to two inferior stabilizers and an upper one)
- It integrates multiple systems for redundancy
- It incorporates an AirSense system capable of detecting aircraft near the UAV
- Its airframe design has an IP45 Ingress Protection

Table 4.9: More features of the selected UAV (*Source:[31]*).

From the characteristics mentioned above, some of them will be further detailed. Taking, for instance, the six-directional positioning system, which is enabled by the vision system and the infrared detection system. While the former gets data from the images that it receives for allowing the exact positioning, the latter uses infrared for detecting obstacles in the drone's way. All the sensors are distributed in the six faces of the vehicle, enhancing the vehicle's response. The combination of both systems even allows the UAV to slow down when obstacles are detected. However, there are some circumstances in which the systems could malfunction, and these should be consulted before flying.

The following Table presents the horizontal and vertical ranges in which obstacles can be detected in both of the mentioned systems.

	Vision System	**Infrared System**
Horizontal Range [m]	0.7-40	0.1-8
Vertical range [m]	0.6-30	0.1-8

Table 4.10: Detection ranges for each system (*Source:[37]*)

Nevertheless, these systems work with sensors, some of which are located at the bottom of the quadrotor, where the payload is attached. In order to properly function, there is an area in which the attached payload should not interfere. The mentioned zone is observable in the figure below.

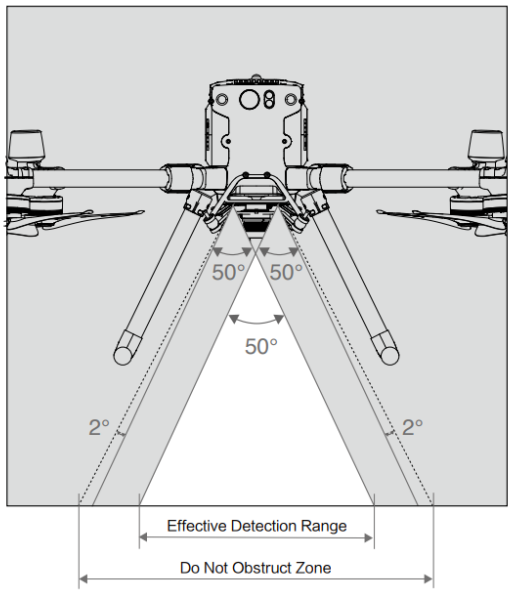

Figure 4.5: Zone that cannot be obstructed (*Source: [37]*).

As it is portrayed, the white area is where the sensors are capable of detecting, and the bigger delimited area, which includes 50 degrees in each border, is the zone that should not be obstructed. This part exactly coincides with where the robotic arm is intended to perform. Therefore, the user's manual of Matrice 300 RTK recommends flying without the vision system since the vehicle could malfunction[37].

Another innovative feature of the UAV is the use of RTK, the acronym is short for *Real Time Kinematic* and stands for a navigation technique capable of improving the use of GNSS. This system uses a fixed station, which can be personalized, so as to wirelessly send corrections to the drone. With this technique, magnetic interferences can be neglected, ensuring flight stability [38, 39].

Maximizing flight safety and reliability is one of the main objectives of this DJI model and that is why redundancy is ensured by having dual flight control sensors, dual control signal links, dual intelligent batteries, dual transmission links, dual obstacle sensor systems, and being able to carry out an emergency landing with three propellers. Having dual flight control sensors means that the vehicle carries two inertial measurement units (IMUs), two barometers, two RTK antennas, two compasses, six vision sensors, and six infrared sensors, allowing the six-direction positioning. More detail about the redundant systems is found in [39].

The last aspect mentioned in Table 4.9 is the airframe's level of protection, which is validated as an IP45 Ingress Protection according to the IEC 60529 standard [37]. The Ingress Protection ratings were developed by the International Electrotechnical Commission (IEC) so as to give an idea of how well electronic equipment resists dust and water. The first number corresponds to the protection against dust on a scale of 0, meaning no protection is ensured, to 6, in which no solid foreign objects interfere. Regarding the second one, it gives an idea of the water resistance, from 0, meaning no protection, to 9, meaning the device is protected from high-pressure hot water from different angles. By having an IP45, the drone is protected from solid objects with a diameter of 1 mm and bigger and protected against water jets [40].

Another aspect that should be considered is the flight modes the UAV has. There are four of them that can be used depending on the pilots' criteria as well as the environmental conditions. The flight modes are:

- **Mode P:** This is the positioning mode, which uses the GNSS system to know its location, stabilize and avoid obstacles. If the GNSS signal is low, the drone uses a barometer to regulate its height.
- **Mode S:** The GNSS system is used for positioning but the drone response improves in terms of speed and becomes more delicate to the controller's actions. It resembles a manual control since the horizontal obstacle detection turns off.
- **Mode T:** This flying mode limits the vehicle's velocity in order to ensure better stability.
- **Mode Atti:** This mode is activated when the visual system does not work or when the GNSS signal is weak. In this, the UAV can not be properly positioned or reduce its velocity. It is the most challenging mode to move the drone.

4.4.2 Components

Some of the essential components of the quadrotor, which numerical parameters are also necessary for the design, are the propulsion system and the batteries. The former is composed by both the DC brushless motors and the propeller. The following Table gives information about which models Matrice 300 RTK uses and some of their fundamental data.

Motor model 6009		**Propeller 2110**		**Batteries TB60**	
Kv [rpm/V]	130	Weight [kg]	0.058	Type	LiPo 12S
Weight [kg]	0.320			Voltage [V]	52.8
ESC maximum voltage	52.2			Energy [Wh]	274

Table 4.11: Components values (*Source:[31]*).

Since the parameters of the propulsion system were not found, a similar propulsion system is considered. Specifically the propulsion system *E2000* from DJI, which uses the motor model 6010 and the propellers of the model 2170 [31].

4.4.3 Design parameters

On the other hand, there will be some numerical values required for computing the control algorithm of the quadrotor. Therefore, some specifications regarding Matrice 300 RTK and its components should be born in mind. In the following Table, the main features are presented.

Quadrotor's numerical features	
Weight (without batteries) [kg]	3.6
Weight (with batteries) [kg]	6.3
Payload max [kg]	2.7
l [m]	0.435

Table 4.12: Numerical Matrice 300 RTK main features (*Source: [31]*).

It should be noted that the last parameter, the length between the motor and the quadrotor's center of mass was determined considering the vehicle's *SOLIDWORKS* model.

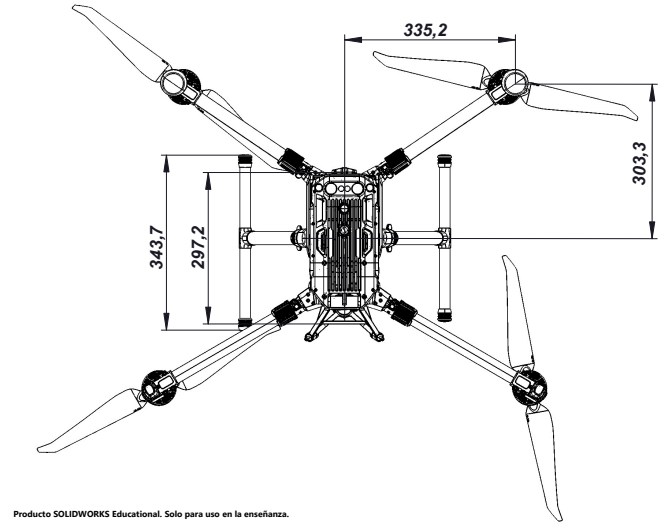

Figure 4.6: Upper view of Matrice 300 RTK blueprint (*Source:[41]*).

From this the length can be obtained by easily computing Pitagora's theorem.

$$l = \sqrt{(335.2)^2 + (303.3)^2} = 452.05 \approx 453\ mm = 0.453\ m$$

Some other values that were not available online are the quadrotor's inertia around each axis. However, they can be approximated by considering the center as a sphere and the rotors as masses located in the distance l of the center [42].

$$I_{xx} = \frac{2}{5} M_{sphere} r^2 + 2l^2 M_{rotor} \tag{4.1}$$

$$I_{yy} = \frac{2}{5} M_{sphere} r^2 + 2l^2 M_{rotor} \tag{4.2}$$

$$I_{zz} = \frac{2}{5} M_{sphere} r^2 + 4l^2 M_{rotor} \tag{4.3}$$

The mass of the whole rotor corresponds to the sum of the motor, the electronic speed controllers, and the

propellers. Taking the values presented in Table 4.11:

$$M_{rotor} = m_{motor} + m_{esc} + m_{propeller} = 0.230 + 0.090 + 0.058 = 0.378\ kgg$$

For computing the sphere's mass, the rotors' mass is subtracted from the drone's total mass. Regarding the radius, it will be considered as the mean value of the three distances (length, height, and width) of the mass located at the center.

$$M_{sphere} = 6.3 - 4 \cdot 0.378 = 4.788\ kg$$

$$r = \frac{297.2 + 146.9 + 209.4}{3} = 217.8\ mm = 0.218\ m$$

Finally, by substituting these results in Equation (4.3), Matrice 300 RTK inertias around each axis result in:

$$I_{xx} = 0.246\ kg \cdot m^2 \qquad I_{yy} = 0.246\ kg \cdot m^2 \qquad I_{zz} = 0.401\ kg \cdot m^2$$

4.5 Regulations

The Easy Access Rules for Unmanned Aircraft Systems, which contains EU Regulations 2019/247 (947) and 2019/945, is the regulation that establishes the UAVs framework for civil drones in Europe. Moreover, acceptable means of compliance (AMC) and guidance material (GM) related to the subject have also been published. This regulation is only applied to outdoor operations [43, 44, 45].

4.5.1 Delegated Regulation (UE) 2019/945

- Defines the requirements for designing and manufacturing UAS.
- Defines the UAS classification.
- Establishes the standards for commercializing the UAS of the open category.
- Establishes the standards for the operators that are not from states that take part in EASA.

The most recent modification of such regulation is the *Delegated Regulation (UE) 2020/1058.*

4.5.2 Implementation Regulation (UE) 2019/947

- Establishes the standards of the use of UAS
- Defines the regulations for the pilots and the organizations

The most recent modification of such regulation is the *Implementation Regulation (UE) 2021/1166.*

4.5.3 Operations categories

Taking the previous regulations into account, UAS are divided into three main categories considering their operations:

- **Open operations:** Low-risk operations. No authorization or declaration has to be made by the operator before using the UAS.
- **Specific operations:** Risky operations that require authorization of the competent authority or a standard scenario statement (STS).
- **Certified operations:** High-risk operations that are regulated in a similar way to traditional aviation.

Open category

This category involves most of the operations carried out. The flight requirements are:

- The UAV must always remain in the pilot's sight (VLOS flight). There are exceptions when the UAS is in *follow-me mode* or another observer is used.
- The UAV cannot fly above 120 m from the surface. In case there is an obstacle of a height higher than 105 m, a flight 15 m above the object's surface is allowed.
- Was the drone to be near a manned aircraft, its flight height should be reduced to land.
- Flying above concentrations of people is not allowed.
- Was an observer to be used, it should be located near the pilot.
- The transportation of dangerous goods or dropping any object is forbidden.

More specific requirements are set for the existing subcategories, which are detailed below together with a summary of what each subcategory considers:

- *A1:* flying over people but not concentrations.
- *A2:* flying close to people.
- *A3:* flying far from people.

Depending on the subcategory of a certain operation, one model of UAV or another can be used. For flying in the open category, there are some crucial features that all these drones have, which are detailed below.

General open category UAVs characteristics
- The maximum fly height is 120 m
- Safely controllable and maneuverable
- Designed to avoid harming people
- Electric
- Commercialized with the manufacturer's instructions

Nevertheless, there are some specific features that should be met for operating in each subcategory. Tables 4.13 and 4.14 gather the identification of the drones, their added characteristics, as well as in which subcategory they can be operated.

A1		**A2**
C0	*C1*	*C2*
Maximum weight 250 g	Maximum weight 900 g Max. impact energy of 80J	Maximum weight 4 kg
Maximum speed 19 m/s	Maximum speed 19 m/s	Minimum speed 3 m/s
	Geo-awareness system	Geo-awareness system
	Controllability lights	Controlability lights
	Back-to-home	Back-to-home
	Identification (serial number)	Identification (serial number)
	Remote identification	Remote identification
		Encripted data so as to avoid interferences

Table 4.13: A1 and A2 subcategories UAVs' features.

A3	
C3	*C4*
Maximum weight 25 kg	Maximum weight 25 kg
Geo-awareness system	It cannot be autonomously flown unless for stabilizing or when the connexion is lost
Controlability lights	
Back-to-home	
Identification (serial number)	
Remote identification	
Encripted data so as to avoid interferences	
Maximum diameter 3 m	

Table 4.14: A3 subcategory UAVs' features.

Specific category

This category corresponds to all the operations that cannot be considered either open or certified. Some examples are:

- When the operation is beyond the visual line of sight.
- When the UAVs' MTOW is higher than 25 kg, which is the maximum weight of the heaviest identification in open operations.

- When the flight has to take place in heights higher than "120 m, the maximum in open operations.
- When the operation requires the dropping of something.
- When the operation takes place in an urban environment with an MTOW lower than 4 kg or the UAV does not have any identification.

In this case of operations, an operator needs to be registered, it could be an agency or the drone's pilot. For performing a specific operation there are four possible scenarios:

- The operation is like an STS. Then, the operator must send a statement of responsibility to the state's authority.
- The operation is performed by a certified-low-UAS-operator capable of authorizing its own operations.
- The operation takes place in clubs where some aero models are authorized.
- The operation does not resemble any STS. The operator must request the state's authority for operational authorization together with a risk evaluation. Only when the authority approves the operation it can be conducted.

Nowadays, there exist two European standard scenarios *STS-01* and *STS-02*, and two national STS in Spain *STS-ES-01* and *STS-ES02*.

Moreover, *Guidance Material Article 3 Categories of UAS operations*, from the *Implementing Regulation (EU) 2019/947* states that a fully autonomous UAS is also considered a specific category.

Certified category

The procedures defined as a certified category are:

- Flights above concentrations of people with a UAS of a bigger diameter than 3 m.
- People transportation.
- Dangerous goods transportation.

4.5.4 Project's regulations

The idea is that the UAV ends up being autonomous and does not require a pilot while operating. Hence, it would be a specific operation that does not resemble any STS. Authorization should be requested to the national authority together with an evaluation of the operation safety. The latter should consider the possible risks of the operation and how to deal with them. It should be noted that the UAV could not begin operating until the national authority approves the flight.

What is more, since the UAV is expected to operate in an urban environment the authority's approval to fly an autonomous drone seems rather unlikely. The same procedure with a pilot could be endorsed provided that the pilot is overly cautious not only due to the possible injuries it could cause but also due to the number of radio interferences a city involves.

Chapter 5

Prototype Design

Having selected the cleaning method along with the payload required, as well as the UAV that would be employed, the design of the final prototype can be elaborated.

5.1 Payload redefinition

Knowing that Matrice 300 RTK is the final drone, its measures have to be considered in order to determine the manipulator's length. Therefore, some of the considerations done in Section 4.2.1 could change, making the redefinition of the payload a must. The following Figure portrays some of the UAV's measurements that should be born in mind.

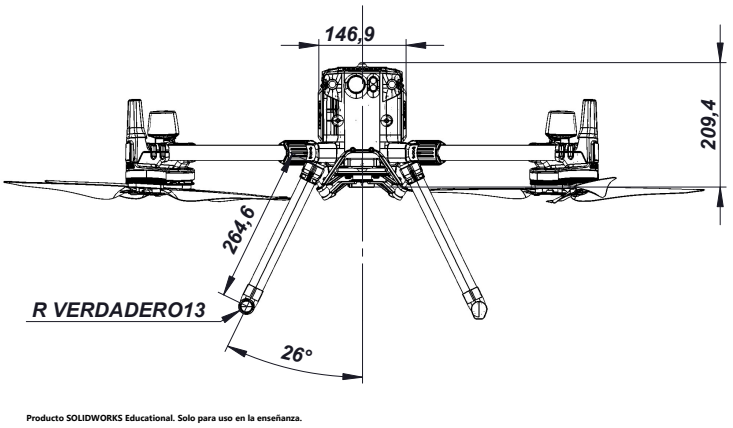

Figure 5.1: Front view of Matrice 300 RTK (*Source: [41]*).

Hence, the minimum length of the arm in order to be capable of touching the panel is equal to the landing gear plus the radius of its ends length.

$$l_{m,minimum} = length + radius \cdot cos(\alpha) = (264.6 + 13) \cdot cos(26) = 249.5\ mm$$

Nevertheless, if this distance was selected, the manipulator could not change its initial position, since the landing gear would hit the panel. Moreover, the benefit of implementing a manipulator is that the mop could autonomously move some degrees, hence, the final length is:

$$l_m = 320\ mm = 0.32\ m$$

Taking α as the angle between axis-x, in which rotor number 1 is located, and the manipulator. When the manipulator does not move, its value is set to be $\frac{-\pi}{2}$ to avoid having a torque (the negative value will be clarified when the frames of the vehicle are detailed). Some limits are established to the angle so as to avoid possible contacts between the manipulator and the quadrotor's landing gear (the big angle is given) or between the landing gear and the panel (the small angle).

$$-1.02\ rad < \alpha < -2.12\ radrad$$

Besides this limit, since the payload in the actual UAV is located at a certain distance from Matrice 300 RTK's center of mass, the whole prototype can land safely by reducing the mop angle.

Hereafter, the actual weight can be computed by doing a linear regression of the weights and lengths of the manipulators consulted in the literature [24, 25, 26, 27].

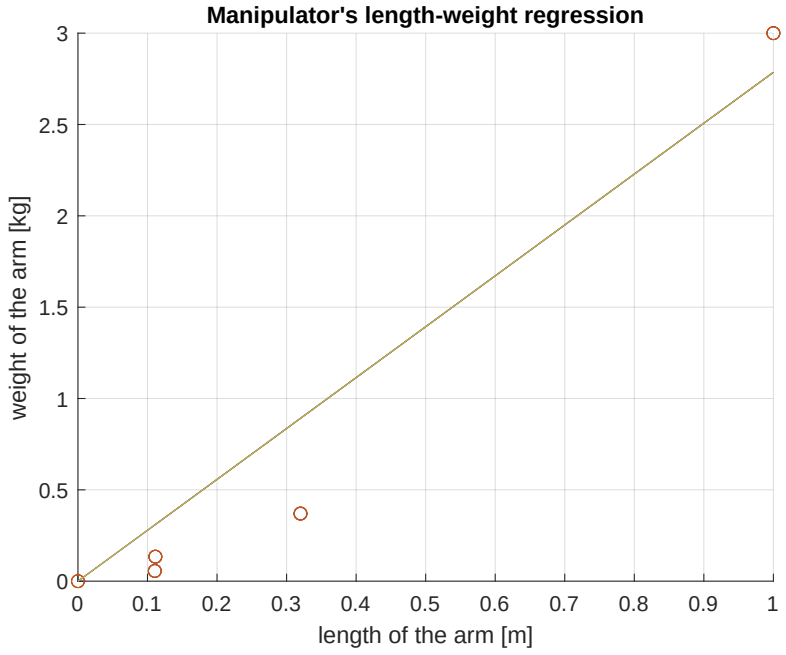

Figure 5.2: Linear regression of the consulted literature manipulators.

While the dots in the Figure above represent the models taken from the literature, the line is the linear regression. The expression that represents the arm's weight as a function of its length is:

$$m_{arm} = 2.786 \cdot l_m \tag{5.1}$$

Introducing in Equation (5.1) the previously defined length of 0.29 m, the mass results in:

$$m_{arm} = 0.891\ kg$$

Therefore, the values in Table 4.2 in Section 4.2.1 should be redefined without exceeding the maximum weight of 1 kg or exceeding it the minimum possible. Then, a linear regression with the length of some mops and their values [28] is done, and attached in Figure 5.3, giving the equation:

$$m_{mop} = 0.791 \cdot l_{mop}$$

The smaller most commonly used solar panels on rooftops are 60-cells panels, which measure 1 $m \times 1.68\ m$ [46], thus, the bigger the mop, the less time the drone spends cleaning one cell. This size relation plays also a role in the mop definition, and it is illustrated together with the linear regression hereafter.

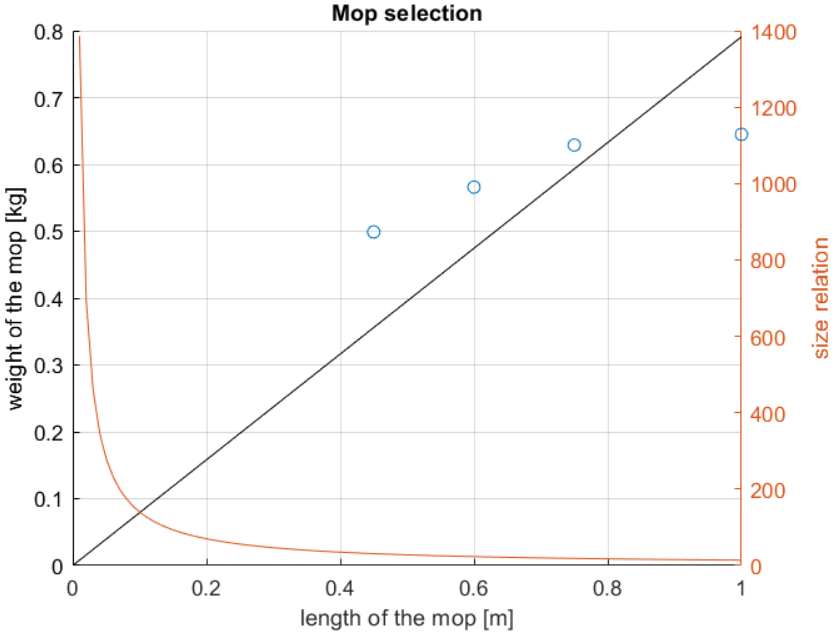

Figure 5.3: Graphics considered for the selection of the mop.

Finally, the selected mop has a of length 0.25 m and a width of 0.12 m, which means that also has a mass of 0.198 kg. The following Table indicates the final weight of each part of the UAV's payload.

Payload	**Weight [kg]**
Robotic arm	0.891
Mop	0.198
Microfiber cloth	0.0074
Total	**1.096**

Table 5.1: Payload final weights.

Once again, the value of the microfiber cloth has been found online in [29]. An extra weight for the manipulator's DC motor is not added since it is involved in the total robotic arm's mass. The weight of the total definitive payload exceeds a little the previously imposed maximum weight. However, since it is a slight difference, some rearrangements could be made so that the total payload's mass is still taken as 1 kg.

5.2 Payload design

The next step in the design is to start shaping the payload components, meaning the joining piece, the manipulator, and the mop. It should be noted that the design achieved is just a first approach to the final one, modifications and improvements will be implemented before getting the definitive design. Figures 5.5, 5.6, and 5.7 are extracted from the project's blueprints, they can be better analyzed in the corresponding document.

5.2.1 Joining piece

Starting with the joining piece, it will be added to the quadrotor's payload piece. The latter is designed so that the UAV can carry up to two cameras attached to it. A zoom in the joining piece of the quadrotor is made and portrayed in Figure 5.4 in order to be able to define the piece that will be linked to the manipulator.

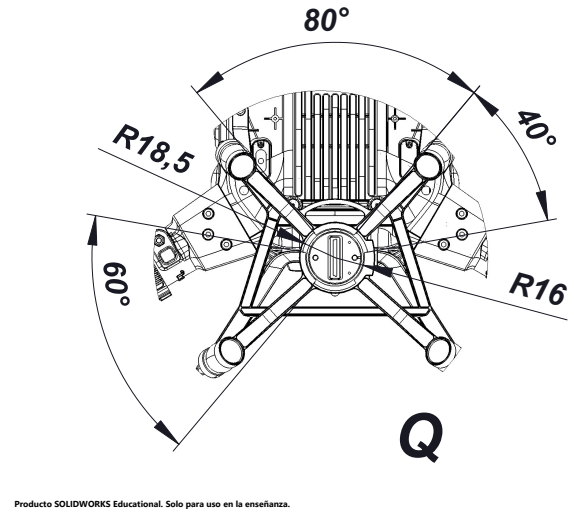

Figure 5.4: Quadrotor joint for the payload (*Source:[41]*).

While the previous measurements will be considered for the upper part of the joining piece, the battery that actions the arm plays also a role in the layout since it should be attached to this piece. Although the used motor should be a servomotor, the exact type is not discussed in the present report. In order to have an approximation, the dimensions of one servomotor capable of moving 1 kg of mass at 17 cm of its shaft are taken. Precisely, the model used is HD-1501MG, and its dimensions are $40.7 \times 20.5 \times 39.5$ mm [47].

The piece will, therefore, consist of two thin walls attached to a base with the exact shape as the joint in Figure 5.4. Both of the walls will have a circumference that connects the servomotor shaft with the

manipulators, the diameter of which is assumed to be 15 mm (it could vary once the motor is chosen). A first impression of how would the joining piece look is attached below.

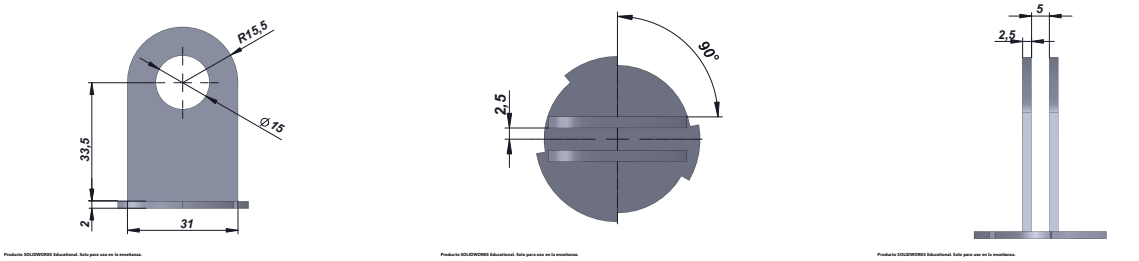

(a) Front view (b) Upper view (c) Lateral view

Figure 5.5: Joining piece views.

The base could be widened and perfectionated by more detailed observation of the quadrotor's joint zoomed in Figure 5.4.

5.2.2 Manipulator

While the manipulator's length has been previously determined in Section 5.1, its width is limited by the walls of the joining's piece, which width is also constrained by the joining's piece base. Since the arm only requires a two-dimensional movement, a simple bar will be used. Two circumferences are emptied so as to enable the joint with the mop as well as for connecting the arm with the servomotor. Since both circles are given the same size, an extra piece (not developed) will be needed for joining the mop and the manipulator. The following Figure gives an initial idea of how this component will be.

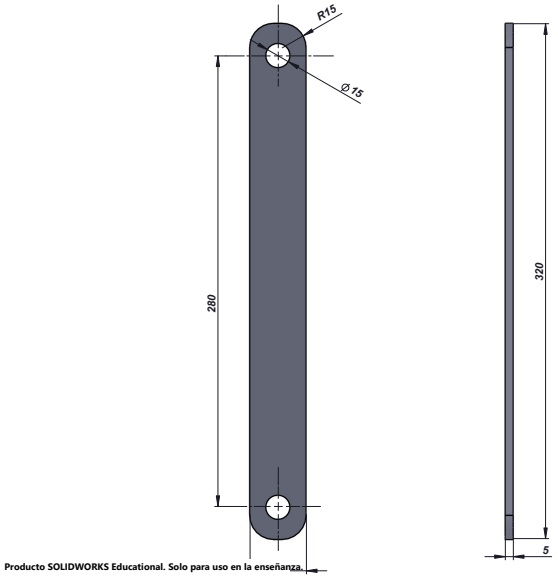

Figure 5.6: Manipulator.

5.2.3 Mop

Finally, the equipment in charge of the actual cleaning, the mop, is also designed following the measurements specifications of Section 5.1. Furthermore, two thin walls similar to the ones of the joining piece are attached for linking the manipulator with the mop.

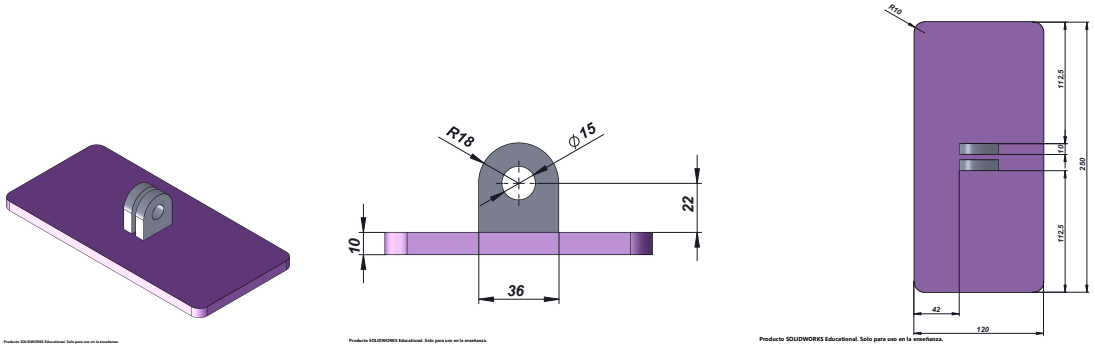

(a) General view (b) Lateral view (c) Upper view

Figure 5.7: Mop views.

5.3 Final configuration

Once all the components have been detailed, all of them are assembled together with the Matrice 300 RTK in a *SOLIDWORKS* assembly. While the joining piece is fixed to the quadrotor, the other components are given one degree of freedom.

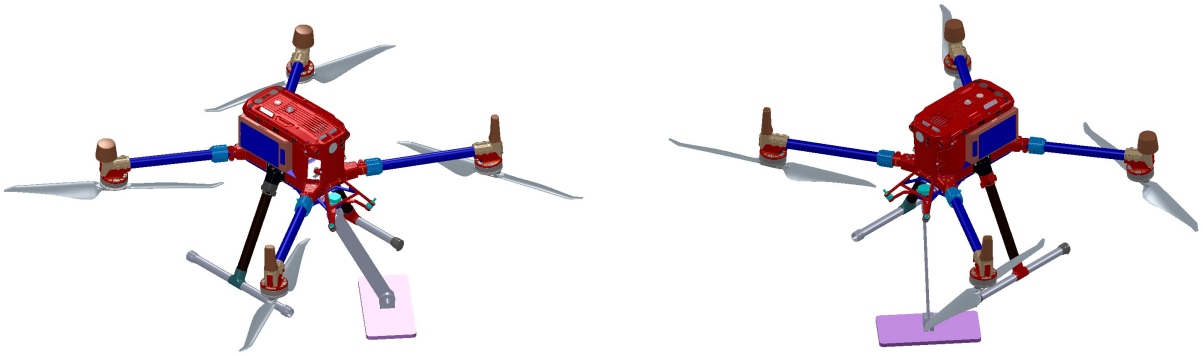

Figure 5.8: Final drone.

To emphasize the fact that a safe landing is ensured in the actual design, it is demonstrated via the prototype assembly of *SOLIDWORKS*. The following Figure portrays the front and upper view of the UAV, in which this position viability is observable since the mop does not hit the landing gear.

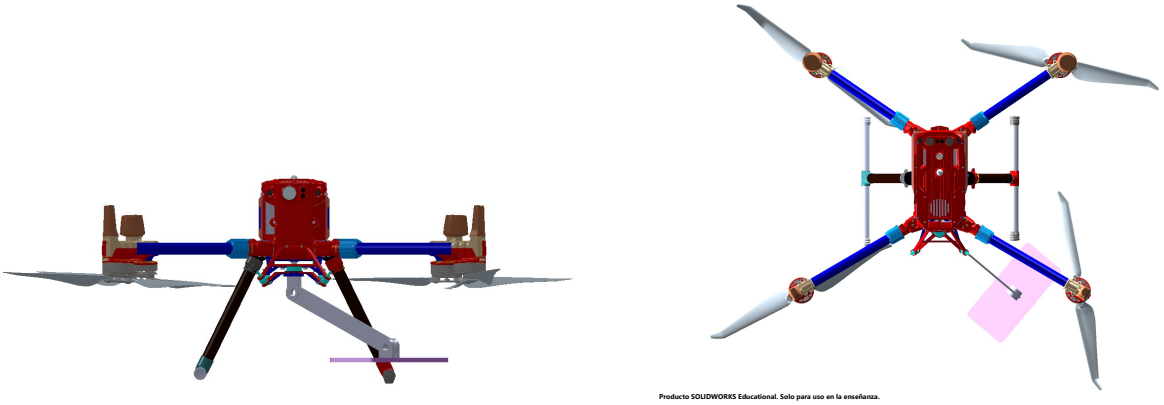

Figure 5.9: Landed final drone.

The obtained prototype is just an initial model to work with, improvements and more detailed components should be designed before mounting the definitive model.

Chapter 6

Mathematical modelling

6.1 Quadrotor modelling

In order to define the modeling of the quadrotor, some assumptions should be born in mind [48, 49]:

1. The center of mass and the body frame origin are at the same point.
2. The body-frame axes are the principal axes of inertia
3. A rigid and symmetrical body is considered.

Moreover,the two different frames used are the Earth inertial reference frame and the body reference frame. Both of them can be observed in the Figure below.

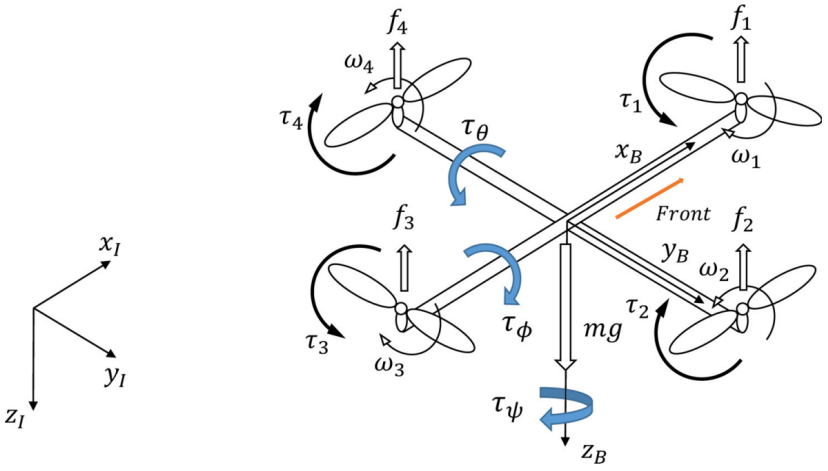

Figure 6.1: Frame's definition (*Source:[50]*).

First and foremost, the vectors regarding position should be defined. The translational position, which is represented with vector $\mathbf{x}$, and the Euler angles, defined as Θ, are expressed in the Earth's inertial frame. Their components are:

$$\mathbf{x} = \begin{bmatrix} x & y & z \end{bmatrix}^T$$

$$\Theta = \begin{bmatrix} \phi & \theta & \psi \end{bmatrix}^T$$

Once the position has been taken care of, the velocity in the same frame can be established deriving the previous vectors with respect to time.

$$\dot{\mathbf{x}} = \begin{bmatrix} \dot{x} & \dot{y} & \dot{z} \end{bmatrix}^T \qquad \dot{\Theta} = \begin{bmatrix} \dot{\phi} & \dot{\theta} & \dot{\psi} \end{bmatrix}^T$$

Nevertheless, it is possible to set the translational and rotational velocities in the body frame, $\mathbf{V}$ and ω respectively.

$$V = \begin{bmatrix} u & v & w \end{bmatrix}^T$$

$$\omega = \begin{bmatrix} p & q & r \end{bmatrix}^T$$

The model is divided into two parts: the kinematics of the UAV and its dynamics.

6.1.1 Quadrotor kinematics

When it comes to the kinematics model, it involves the relation of velocities between the two possible frames used (the inertial and the body frame) [27]:

$$\omega = R_r \dot{\Theta} \tag{6.1}$$

$$\dot{\mathbf{x}} = RV \tag{6.2}$$

In which ω and V are the velocities expressed in the body frame and the velocities in $\dot{\Theta}$ and $\dot{\mathbf{x}}$ are related to the Earth's inertial frame. Before defining any rotational matrix (R_r, R), the matrices that define the rotation along each axis should be born in mind.

$$R_\phi = \begin{bmatrix} 1 & 0 & 0 \\ 0 & cos(\phi) & sin(\phi) \\ 0 & -sin(\phi) & cos(\phi) \end{bmatrix} \qquad R_\theta = \begin{bmatrix} cos(\theta) & 0 & -sin(\theta) \\ 0 & 1 & 0 \\ sin(\theta) & 0 & cos(\theta) \end{bmatrix} \qquad R_\psi = \begin{bmatrix} cos(\psi) & sin(\psi) & 0 \\ -sin(\psi) & cos(\psi) & 0 \\ 0 & 0 & 1 \end{bmatrix}$$

Then, assuming a small time derivative of each Euler rate, the matrix R_r, which relates the angular velocities

in the body frame with the inertial frame is defined as [51, 52]:

$$\begin{bmatrix} p \\ q \\ r \end{bmatrix} = \begin{bmatrix} \dot{\phi} \\ 0 \\ 0 \end{bmatrix} + R_\phi \begin{bmatrix} 0 \\ \dot{\theta} \\ 0 \end{bmatrix} + R_\phi R_\theta \begin{bmatrix} 0 \\ 0 \\ \dot{\psi} \end{bmatrix}$$

The procedure followed for obtaining the rotational matrix (R_r) consists on rotating the Earth inertial frame ($x_E = x_1$) until the body frame is reached (x). Starting backwards, the last rotation is around x_3, meaning that the angle involved is $\dot{\phi}$. Then, the axis is rotated around $y_2 = y_3$, having a variation in $\dot{\theta}$, and lastly the movement is around $z_2 = z_1$, being $\dot{\psi}$ the change affected. The whole process can be observed in the Figure below.

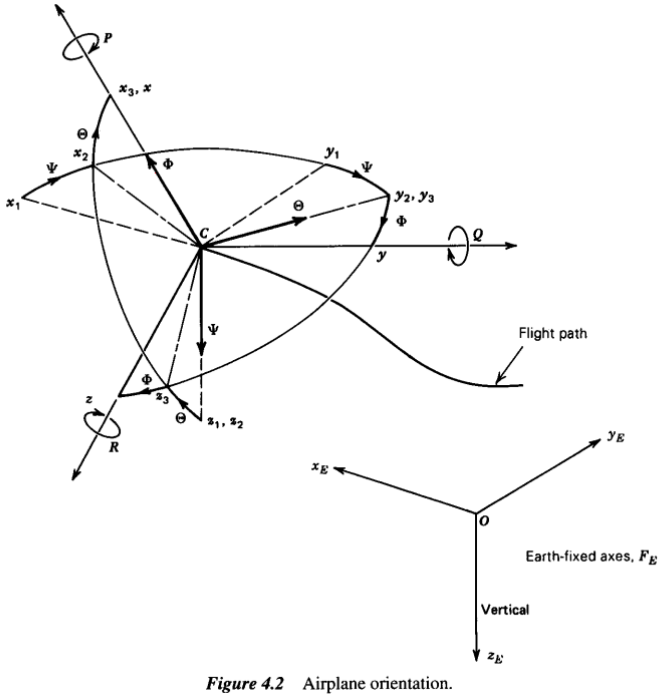

Figure 4.2 Airplane orientation.

Figure 6.2: Euler angles related to Earth's fixed frame (*Source:[52]*).

Finally, the rotation matrix results in :

$$R_r = \begin{bmatrix} 1 & 0 & -sin\theta \\ 0 & cos\phi & sin\phi cos\theta \\ 0 & -sin\phi & cos\phi cos\theta \end{bmatrix}$$

On the other hand, the rotation matrix R, which relates the translational velocities of the body frame with

the inertial, is computed by the consideration of the rotations required along each axis in the order: roll, pitch and finally yaw.

$$R = \begin{bmatrix} cos\theta cos\psi & sin\phi sin\theta cos\psi - sin\psi cos\phi & cos\phi sin\theta cos\psi + sin\phi sin\psi \\ cos\theta sin\psi & sin\phi sin\theta sin\psi + cos\phi cos\psi & cos\phi sin\theta sin\psi - sin\phi cos\psi \\ -sin\theta & sin\phi cos\theta & cos\phi cos\theta \end{bmatrix} \tag{6.3}$$

6.1.2 Quadrotor dynamics

The dynamics of the UAV are obtained through the Newton-Euler equation, which is defined below in the body frame:

$$\begin{bmatrix} m_{UAV} I_{3\times 3} & 0 \\ 0 & J \end{bmatrix} \begin{bmatrix} \dot{V}^B \\ \dot{\omega}^B \end{bmatrix} + \begin{bmatrix} \omega^B \times (m_{UAV} V^B) \\ \omega^B \times (J_{UAV} \omega^B) \end{bmatrix} = \begin{bmatrix} F^B \\ \tau^B \end{bmatrix} \tag{6.4}$$

In which m_{UAV} and J_{UAV} are resepcively the drone's mass and inertia, and I is the identity matrix. The terms F^B and τ^B correspond to the force and the torque produced in the body-frame. With the aim of easing the procedure, the equation will be separated into two parts: one related to the translational movements and the other with the rotational ones. Starting with the translational equation, it corresponds to the first row of Equation (6.4):

$$mI_{3\times 3}\dot{V}^B + \omega^B \times (mV^B) = F^B$$

Substituting the vectors V and ω by its already defined components, the equation can be rewritten as [53]:

$$\begin{bmatrix} \dot{u} \\ \dot{v} \\ \dot{w} \end{bmatrix} + \begin{bmatrix} qw - vr \\ ru - pw \\ pv - uq \end{bmatrix} = \frac{1}{m_{UAV}} \begin{bmatrix} f_x \\ f_y \\ f_z \end{bmatrix}$$

The force vector has been divided into its main components, however, these need to be defined. One of the forces that the vehicle has is the gravity one (F_g), which is located in the center of mass. Being a symmetric body, the latter is in the center of the drone. Moreover, the force is perpendicular to Earth, meaning it has a component in the *z-axis* of the Earth inertial frame. Since Equation (6.1.2) is defined in the Body-frame, the rotational matrix R, expressed in Equation (6.3) is required.

$$F_g^B = R^T \begin{bmatrix} 0 \\ 0 \\ m_{UAV}g \end{bmatrix} = \begin{bmatrix} -m_{UAV}gsin\theta \\ m_{UAV}gcos\theta sin\phi \\ m_{UAV}gcos\theta cos\phi \end{bmatrix}$$

Another acting force is the thrust produced by the four propellers (F_p), which has an effect in the *z-axis* of the body frame.

$$F_p^B = \begin{bmatrix} 0 \\ 0 \\ -(T_1 + T_2 + T_3 + T_4) \end{bmatrix}$$

Supposing that there is no influence of the aerodynamic forces, meaning that drag is neglected, the force vector results:

$$F^B = F_g^B + F_p^B = \begin{bmatrix} -m_{UAV}gsin(\theta) \\ m_{UAV}gcos\theta sin\phi \\ -(T_1 + T_2 + T_3 + T_4) + m_{UAV}gcos\theta cos\phi \end{bmatrix} \tag{6.5}$$

Hence, all the components of Equation (6.1.2) have been computed.

Regarding the rotational equation of motion of the quadrotor, which corresponds to the second row:

$$J_{UAV}\dot{\omega}^B + \omega^B \times (J_{UAV}\omega^B) = \tau^B \tag{6.6}$$

Since the UAV was supposed to be a symmetric structure the inertias $I_{xy} = I_{yx} = I_{xz} = I_{zx} = I_{yz} = I_{zy} = 0$, which simplifies the expression. Substituting vector ω by its components, it is redefined as:

$$\begin{bmatrix} \dot{p} \\ \dot{q} \\ \dot{r} \end{bmatrix} + \begin{bmatrix} \frac{(I_{zz}-I_{yy})}{I_{xx}}qr \\ \frac{I_{xx}-I_{zz})}{I_{yy}}pr \\ \frac{(I_{yy}-I_{xx})}{I_{zz}}pq \end{bmatrix} = \begin{bmatrix} \frac{1}{I_{xx}}\tau_\phi \\ \frac{1}{I_{yy}}\tau_\theta \\ \frac{1}{I_{zz}}\tau_\psi \end{bmatrix}$$

The torque vector has been divided into its main components, which have to be computed. The thrust generated by each propeller produces a momentum that influences a specific rotation. Furthermore, the yaw rotation (ψ) is affected by the momentum that a spinning propeller produces. Being the torques around each

rotation ($\tau_\phi, \tau_\theta, and \tau_\psi$) described as:

$$\tau_\phi = l(T_4 - T_2)$$
$$\tau_\theta = l(T_1 - T_3)$$
$$\tau_\psi = -M_1 + M_2 - M3 + M_4$$

In addition, the thrust and the momentum can be related to the propeller's rotational speed with two different constants, K_f for the thrust and K_M for the torque.

$$T_i = K_f \Omega_i^2$$
$$M_i = K_M \Omega_i^2$$

Meaning that the total momentum produced in the UAV considering each axis as an axis of rotation, in the Body-frame, can be written as:

$$M^B = \begin{bmatrix} lK_f(-\Omega_2^2 + \Omega_4^2) \\ lK_f(\Omega_1^2 - \Omega_3^2) \\ K_M(-\Omega_1^2 + \Omega_2^2 - \Omega_3^2 + \Omega_4^2) \end{bmatrix}$$

However, there are gyroscopic effects that also affect the momentum of the drone. The fact that two of the rotors rotate in the opposite direction of the other two originates a gyroscopic torque when there is a difference in the rotor's speed. In order to identify such difference, the rotors' relative speed Ω_r should be defined.

$$\Omega_r = -\Omega_1 + \Omega_2 - \Omega_3 + \Omega_4$$

Being Ω_i the rotational speed of the propeller i. The gyroscopic effects influence the angles of ϕ and τ as the following equation expresses:

$$M_G = J_p \begin{bmatrix} q\Omega_r \\ p\Omega_r \\ 0 \end{bmatrix}$$

In which J_p is the rotational moment of inertia. The gyroscopic momentum can be introduced in equation (6.6) since the total torque produced in the body can be written as:

$$\tau^B = M^B - M_G = \begin{bmatrix} lK_f(-\Omega_2^2 + \Omega_4^2) - J_p q \Omega_r \\ lK_f(\Omega_1^2 - \Omega_3^2) - J_p p \Omega_r \\ K_M(-\Omega_1^2 + \Omega_2^2 - \Omega_3^2 + \Omega_4^2) \end{bmatrix}$$

Additionaly, the relations between the thrust and the torques can be grouped in the variables U that are stated below.

$$\begin{bmatrix} U_1 \\ U_2 \\ U_3 \\ U_4 \end{bmatrix} = \begin{bmatrix} K_f(\Omega_1^2 + \Omega_2^2 + \Omega_3^2 + \Omega_4^2) \\ lK_f(-\Omega_2^2 + \Omega_4^2) \\ lK_f(\Omega_1^2 - \Omega_3^2) \\ K_M(-\Omega_1^2 + \Omega_2^2 - \Omega_3^2 + \Omega_4^2) \end{bmatrix}$$

Finally, considering Equations (6.1.2) and (6.6) and the matrices expresses above, the quadrotor's dynamic equations result in:

$$\begin{cases} \dot{u} = vr - qw - gsin\theta \\ \dot{v} = pw - ru + gcos\theta sin\phi \\ \dot{w} = uq - pv + gcos\theta cos\phi - \frac{U_1}{m_{UAV}} \\ \dot{p} = \frac{I_{yy} - I_{zz}}{I_{xx}} qr - \frac{J_p \Omega_r q}{I_{xx}} + \frac{U_2}{I_{xx}} \\ \dot{q} = \frac{I_{zz} - I_{xx}}{I_{yy}} pr - \frac{J_p \Omega_r p}{I_{yy}} + \frac{U_3}{I_{yy}} \\ \dot{r} = \frac{I_{xx} - I_{yy}}{I_{zz}} pq + \frac{U_4}{I_{zz}} \end{cases}$$

Nevertheless, for modeling a hybrid frame is actually used. While the linear expressions are in the inertial frame, the angular ones are expressed in the body frame. In order to express Equation (6.1.2) in the Inertial frame, the forces previously defined in the Body-frame should be transformed into the Inertial one.

$$F^E = F_g^E + F_p^E = \begin{bmatrix} 0 \\ 0 \\ mg \end{bmatrix} + R \begin{bmatrix} 0 \\ 0 \\ -U_1 \end{bmatrix} = \begin{bmatrix} -(cos\phi sin\theta cos\psi + sin\phi sin\psi)U_1 \\ -(cos\phi sin\theta sin\psi - sin\phi cos\psi)U_1 \\ -cos\phi cos\theta U_1 + mg \end{bmatrix}$$

Moreover, vectors V and ω should be respectively replaced by $\dot{x}$ and Θ. Therefore, the final equations that describe the dynamic response of the drone are:

$$\begin{cases} \ddot{X} = -(cos\phi sin\theta cos\psi + sin\phi sin\psi)\frac{U_1}{m_{UAV}} \\ \ddot{Y} = -(cos\phi sin\theta sin\psi - sin\phi cos\psi)\frac{U_1}{m_{UAV}} \\ \ddot{Z} = -cos\phi cos\theta \frac{U_1}{m_{UAV}} + g \\ \dot{p} = \frac{I_{yy} - I_{zz}}{I_{xx}} qr - \frac{J_p \Omega_r q}{I_{xx}} + \frac{U_2}{I_{xx}} \\ \dot{q} = \frac{I_{zz} - I_{xx}}{I_{yy}} pr - \frac{J_p \Omega_r p}{I_{yy}} + \frac{U_3}{I_{yy}} \\ \dot{r} = \frac{I_{xx} - I_{yy}}{I_{zz}} pq + \frac{U_4}{I_{zz}} \end{cases} \tag{6.7}$$

6.2 Quadrotor with a manipulator

In this section, the modeling of the quadrotor equipped with a robotic arm is developed. To do so, there are some assumptions that should be taken into account.

- The manipulator only moves in the x-z plane.
- The manipulator is attached to the quadrotor's center of mass, therefore, the vehicle's Body-frame can be easily related to the arm's frame.
- All the payload (including the mop) is referred as the manipulator and it is contemplated as a bar of 1 kg (m_{PL}) and length of 0.32 m (l_m).
- The angle between the positive x-axis and the manipulator is α, and its initial value is $\frac{-\pi}{2}$

For computing the quadrotor's control, the effects of the manipulators' in the drone have to be born in mind [54]. The forces and moments produced by the manipulator on the quadrotor are computed in the following subsections.

6.2.1 Manipulator forces

Since the quadrotor model in Equation (6.7) uses both the Inertial and Body frame, the forces of the manipulator are determined in the two frames. On the one hand, the robotic arm has a gravitational force due to its mass. This is located at the manipulator's center of mass and always points in the z-direction of the Inertial frame.

$$F^I_{PL,g} = \begin{bmatrix} 0 \\ 0 \\ m_{PL}g \end{bmatrix} \qquad F^B_{PL,g} = R^T \begin{bmatrix} 0 \\ 0 \\ -m_{PL}g \end{bmatrix} = \begin{bmatrix} -m_{PL}gsin\theta \\ m_{PL}gcos\theta sin\phi \\ m_{PL}gcos\theta cos\phi \end{bmatrix}$$

On the other hand, the other force that will be evaluated is the centrifugal force. It corresponds to the resistance that the arm has to follow a circular path. Some variables are introduced: the angular velocity of the center of mass ω_m (which can is related to $alpha$ as $w_m = \frac{d\alpha}{dt}$) and the distance between the center of mass and the origin r.

$$F^I_{PL,c} = R \begin{bmatrix} -m_{PL}\omega_m^2 r \\ 0 \\ 0 \end{bmatrix} = \begin{bmatrix} -m_{PL}\omega_m^2 rcos\theta cos\psi \\ -m_{PL}\omega_m^2 rcos\theta sin\psi \\ m_{PL}\omega_m^2 rsin\theta \end{bmatrix} \qquad F^B_{PL,c} = - \begin{bmatrix} m_{PL}\omega_m^2 r \\ 0 \\ 0 \end{bmatrix}$$

The distance between the origin and arm's center of mass corresponds to half the length of the manipulator $\frac{l_m}{2}$. All the other forces, such as the resistance, and the Euler forces are supposed negligible. Then, the total

force produced by the manipulator in the inertial frame is the sum of the previously described forces.

$$F_{PL}^{I} = \begin{bmatrix} 0 \\ 0 \\ m_{PL}g \end{bmatrix} + \begin{bmatrix} -m_{PL}\omega_m^2 \frac{l_m}{2} cos\theta cos\psi \\ -m_{PL}\omega_m^2 \frac{l_m}{2} cos\theta sin\psi \\ -m_{PL}\omega_m^2 \frac{l_m}{2}(-sin\theta) \end{bmatrix} = \begin{bmatrix} -m_{PL}\omega_m^2 \frac{l_m}{2} cos\theta cos\psi \\ -m_{PL}\omega_m^2 \frac{l_m}{2} cos\theta sin\psi \\ m_{PL}\omega_m^2 \frac{l_m}{2} sin\theta) + m_{PL}g \end{bmatrix}$$

These results can be added to the translational expressions of Equation (6.7), which are also expressed in the Inertial frame. Finally, the translational expressions for the system are:

$$\begin{cases} \ddot{X} = -(cos\phi sin\theta cos\psi + sin\phi sin\psi)\frac{U_1}{m} - \frac{m_{PL}}{m}\omega_m^2 \frac{l_m}{2} cos\theta cos\psi \\ \ddot{Y} = -(cos\phi sin\theta sin\psi - sin\phi cos\psi)\frac{U_1}{m} - \frac{m_{PL}}{m}\omega_m^2 \frac{l_m}{2} cos\theta sin\psi \\ \ddot{Z} = -cos\phi cos\theta \frac{U_1}{m} + \frac{m_{PL}}{m}\omega_m^2 \frac{l_m}{2} sin\theta + g(1 + \frac{m_{PL}}{m}) \end{cases} \tag{6.8}$$

6.2.2 Manipulator moments

Not only do these forces influence the translational movement of the quadrotor, but they also produce torque. In this case, however, the UAV's rotational expressions are based in the Body frame. Hence, for computing the moments, the forces in the latter frame are taken. When it comes to the moment of the gravitational force:

$$M_{PL,g} = F_{PL,g}^{B} \times r_m = \begin{bmatrix} -m_{PL}gsin\theta \\ m_{PL}gcos\theta sin\phi \\ m_{PL}gcos\theta cos\phi \end{bmatrix} \times \begin{bmatrix} \frac{l_m}{2} cos(\alpha) \\ 0 \\ \frac{l_m}{2} sin(\alpha) \end{bmatrix} = \begin{bmatrix} m_{PL}gcos\theta sin\phi \frac{l_m}{2} sin(\alpha) \\ m_{PL}g\frac{l_m}{2}(sin\theta sin(\alpha) + cos\theta cos\phi cos(\alpha)) \\ -m_{PL}gcos\theta sin\phi \frac{l_m}{2} cos(\alpha) \end{bmatrix}$$

Being α the angle between the manipulator and the x-axis. Regarding the moment produced by the centrifugal force, the expression taken into account is detailed below.

$$M_{PL,c} = F_{PL,c}^{B} \times r_m = \begin{bmatrix} m_{PL}\omega_m^2 \frac{l_m}{2} \\ 0 \\ 0 \end{bmatrix} \times \begin{bmatrix} -\frac{l_m}{2} cos(\alpha) \\ 0 \\ \frac{l_m}{2} sin(\alpha) \end{bmatrix} = \begin{bmatrix} 0 \\ +m_{PL}\omega_m^2 \frac{l_m}{2} \frac{l_m}{2} sin(\alpha) \\ 0 \end{bmatrix}$$

The same way it was done with the forces, the total moment produced by the manipulator corresponds to the sum of the moments created by both of the considered forces.

$$M_{PL}^{B} = M_{PL,g} + M_{PL,c} = \begin{bmatrix} m_{PL}gcos\theta sin\phi \frac{l_m}{2} sin(\alpha) \\ m_{PL}g\frac{l_m}{2}(sin\theta sin(\alpha) + cos\theta cos\phi cos(\alpha)) + m_{PL}\omega_m^2 \frac{l_m}{2}\frac{l_m}{2} sin(\alpha) \\ -m_{PL}gcos\theta sin\phi \frac{l_m}{2} cos(\alpha) \end{bmatrix}$$

Taking the rotational expressions from Equation (6.7) and adding the new moments computed, the new model is:

$$\begin{cases} \dot{p} = \frac{I_{yy}-I_{zz}}{I_{xx}} qr - \frac{J_p\Omega_r q}{I_{xx}} + \frac{U_2}{I_{xx}} + \frac{m_{PL}gcos\theta sin\phi \frac{l_m}{2} sin(\alpha)}{I_{xx}} \\ \dot{q} = \frac{I_{zz}-I_{xx}}{I_{yy}} pr - \frac{J_p\Omega_r p}{I_{yy}} + \frac{U_3}{I_{yy}} + \frac{m_{PL}g\frac{l_m}{2}(sin\theta sin(\alpha)+cos\theta cos\phi cos(\alpha))+m_{PL}\omega_m^2\frac{l_m}{2}\frac{l_m}{2}sin(\alpha)}{I_{yy}} \\ \dot{r} = \frac{I_{xx}-I_{yy}}{I_{zz}} pq + \frac{U_4}{I_{zz}} - \frac{m_{PL}gcos\theta sin\phi \frac{l_m}{2} cos(\alpha)}{I_{zz}} \end{cases} \tag{6.9}$$

6.2.3 System equation

The resulting equation is a combination of Equations (6.8) and (6.9), which actually are a modification of Equation (6.7).

$$\begin{cases} \ddot{X} = -(cos\phi sin\theta cos\psi + sin\phi sin\psi)\frac{U_1}{m} - \frac{m_{PL}}{m}\omega_m^2 \frac{l_m}{2} cos\theta cos\psi \\ \ddot{Y} = -(cos\phi sin\theta sin\psi - sin\phi cos\psi)\frac{U_1}{m} - \frac{m_{PL}}{m}\omega_m^2 \frac{l_m}{2} cos\theta sin\psi \\ \ddot{Z} = -cos\phi cos\theta \frac{U_1}{m} + \frac{m_{PL}}{m}\omega_m^2 \frac{l_m}{2} sin\theta + g(1 + \frac{m_{PL}}{m}) \\ \dot{p} = \frac{I_{yy}-I_{zz}}{I_{xx}} qr - \frac{J_p\Omega_r q}{I_{xx}} + \frac{U_2}{I_{xx}} + \frac{m_{PL}gcos\theta sin\phi \frac{l_m}{2} sin(\alpha)}{I_{xx}} \\ \dot{q} = \frac{I_{zz}-I_{xx}}{I_{yy}} pr - \frac{J_p\Omega_r p}{I_{yy}} + \frac{U_3}{I_{yy}} + \frac{m_{PL}g\frac{l_m}{2}(sin\theta sin(\alpha)+cos\theta cos\phi cos(\alpha))+m_{PL}\omega_m^2\frac{l_m}{2}\frac{l_m}{2}sin(\alpha)}{I_{yy}} \\ \dot{r} = \frac{I_{xx}-I_{yy}}{I_{zz}} pq + \frac{U_4}{I_{zz}} - \frac{m_{PL}gcos\theta sin\phi \frac{l_m}{2} cos(\alpha)}{I_{zz}} \end{cases} \tag{6.10}$$

6.2.4 Dynamics of the manipulator

Nevertheless, there is still an equation to be determined so as to relate the new angle α to its derivatives. This equation is the dynamic expression of the manipulator. The procedure followed is similar to the one described in [55], but using one link instead of two. The equation that describes the dynamics of a robotic manipulator is:

$$M(\alpha)\ddot{\alpha} + C(\alpha, \dot{\alpha}) + g(\alpha) = \tau_{PL} \tag{6.11}$$

In which M is the inertia matrix, C is the Coriolis and centrifugal matrix, and g is the potential and gravitational one. Moreover, α is the angle between the link's center of mass and the horizontal, and τ is the torque produced.

For deriving the equation of motion, the Lagrange method is used as in [56]. Being $\mathcal{T}$ the kinetic energy and

$\mathcal{U}$ the potential energy, the Lagrange function can be written as:

$$\mathcal{L} = \mathcal{T} - \mathcal{U} = \frac{1}{2} m_{PL} v_{PL}^2 + \frac{1}{2} I_{PL} w_{PL}^2 - m_{PL} g h$$

The values of v_{PL} and w_{PL} correspond to the translational and angular velocities of the manipulator, while m_{PL} is the sum of the arm's and the mop's mass. In order to obtain the equation of motion, the following expression is used.

$$\frac{d}{dt}\frac{d\mathcal{L}}{d\dot{\alpha_i}} - \frac{d\mathcal{L}}{d\alpha_i} = \tau_i \tag{6.12}$$

Since in this project there is only one link considered, there is only one value of i, thus, the resultant torque is the one produced by the manipulator. τ_i will then be τ_{PL}. The position of the robotic arm's center of mass is given by the vector p. Moreover, deriving such point with respect to time, the velocity v_{PL} can be determined.

$$p = \frac{l}{2}\begin{bmatrix} cos(\alpha) \\ \\ sin(\alpha) \end{bmatrix} \rightarrow v_{PL} = \begin{bmatrix} -\frac{lsin(\alpha)\dot{\alpha}}{2} \\ \\ \frac{lcos(\alpha)\dot{\alpha}}{2} \end{bmatrix}$$

Knowing v_{PL}, it is possible to determine the kinetic energy as $T = \frac{m_{PL} v_{PL}^2}{2} + \frac{I_{PL} w_{PL}^2}{2}$, in which w_{PL} is only affected by the manipulator's angle, being $\dot{\alpha}$. Once T is computed, all the derivatives regarding the kinetic energy in Equation (6.12) can be obtained.

$$\frac{dT}{d\alpha} = 0 \qquad \frac{dT}{d\dot{\alpha}} = \frac{l^2 m_{PL} + \dot{\alpha}}{4} + I_{PL}\dot{\alpha} \qquad \frac{d}{dt}\frac{dT}{d\dot{\alpha}} = \frac{l^2 m_{PL}\ddot{\alpha}}{4} + I_{PL}\ddot{\alpha}$$

On the other hand, the potential energy can also be reached since $U = m_{PL} g h$ in where h is the height of the center of mass; $U = m_{PL} g \frac{lsin(\alpha)}{2}$. Then,

$$\frac{dU}{d\alpha} = \frac{l m_{PL} g cos(\alpha)}{2}$$

Relating the values obtained through the derivatives of the kinetic and potential energy to Equation (6.11), the terms M, C, and g result:

$$M = \frac{m_{PL} l^2}{4} + I_{PL} \qquad C = 0 \qquad g = \frac{m_{PL} l cos(\alpha)}{2}$$

Finally, bearing Equation (6.12) in mind, and with all the previous results determined, the value of the torque generated by the manipulator is:

$$\tau_{PL} = \frac{m_{PL} l^2 \ddot{\alpha}}{4} + I_{PL}\ddot{\alpha} - \frac{m_{PL} g l cos(\alpha)}{2} \tag{6.13}$$

τ_{PL} is expressed in the Body-frame of the manipulator, which is supposed to be the UAV's Body-frame too.

Another variable that needs to be computed is the inertia of the manipulator. The movement of the arm

is supposed to be bi-dimensional, specifically in the axis x and z. Hence, the actual rotation of the arm is around the axis y. For computing the inertia, two procedures can be followed. The first one consists in using the Steiner Theorem, which states that:

$$I = I_{MC} + Md^2$$

I_{MC} corresponds to the inertia supposing that the rotation axis is in the center of mass. Besides, d is the distance between the actual rotation axis and the center of mass. This method is useful when the rotation axis is not located in the studied object.

In this case, nonetheless, the link rotates about its end, meaning that the other way for obtaining the inertia can be computed. To do so, a differential of inertia, which requires a mass differential, has to be determined:

$$dm = \lambda dr = \frac{mdr}{l}$$

Where λ stands for the mass per unit length of the rod. Introducing the mass differential in the inertia computation results in:

$$I = \int r^2 dm = \int r^2 \frac{m}{l} dr$$

Applying the previous expression to each axis, the final inertias computed are [55]:

$$\begin{aligned} I_{x,m} &= \int z^2 dm = \int_0^{lsin(\alpha)} z^2 \frac{m}{l} dz = \left[\frac{mz^3}{3l}\right]_0^{lsin(\alpha)} = \frac{ml^2 sin^3(\alpha)}{3} \\ I_{y,m} &= \int (x^2 + z^2) dm = \int_0^{l} r^2 \frac{m}{l} dr = \left[\frac{r^3 m}{3l} dr\right]_0^{l} = \frac{ml^2}{3} \\ I_{z,m} &= \int x^2 dm = \int_0^{lcos(\alpha)} x^2 \frac{m}{l} dx = \left[\frac{mx^3}{3l}\right]_0^{lcos(\alpha)} = \frac{ml^2 cos^3(\alpha)}{3} \end{aligned} \tag{6.14}$$

It should be highlighted that in the previous Equation (6.14) the mass variable m actually refers to the payload's mass m_{PL}. Since the robotic arm is defined in the xz-plane, the only inertia that will be taken into account is I_{yy}, which is the inertia of the axis the arm rotates around. The other inertias are neglected.

Finally, the combined expressions required for modeling the combination of the UAV and the robotic arm are:

$$\begin{cases} \ddot{X} = -(cos\phi sin\theta cos\psi + sin\phi sin\psi)\frac{U_1}{m} - \frac{m_{PL}}{m}\omega_m^2 \frac{l_m}{2} cos\theta cos\psi \\ \ddot{Y} = -(cos\phi sin\theta sin\psi - sin\phi cos\psi)\frac{U_1}{m} - \frac{m_{PL}}{m}\omega_m^2 \frac{l_m}{2} cos\theta sin\psi \\ \ddot{Z} = -cos\phi cos\theta \frac{U_1}{m} + \frac{m_{PL}}{m_T}\omega_m^2 \frac{l_m}{2} sin\theta + g(1 + \frac{m_{PL}}{m}) \\ \dot{p} = \frac{I_{yy} - I_{zz}}{I_{xx}} qr - \frac{J_p \Omega_r q}{I_{xx}} + \frac{U_2}{I_{xx}} + \frac{m_{PL} g cos\theta sin\phi \frac{l_m}{2} sin(\alpha)}{I_{xx}} \\ \dot{q} = \frac{I_{zz} - I_{xx}}{I_{yy}} pr - \frac{J_p \Omega_r p}{I_{yy}} + \frac{U_3}{I_{yy}} + \frac{m_{PL} g \frac{l_m}{2} (sin\theta sin(\alpha) + cos\theta cos\phi cos(\alpha)) + m_{PL}\omega_m^2 \frac{l_m}{2} \frac{l_m}{2} sin(\alpha)}{I_{yy}} \\ \dot{r} = \frac{I_{xx} - I_{yy}}{I_{zz}} pq + \frac{U_4}{I_{zz}} - \frac{m_{PL} g cos\theta sin\phi \frac{l_m}{2} cos(\alpha)}{I_{zz}} \\ \tau_{PL} = (\frac{m_{PL} l^2}{4} + I_{ym})\ddot{\alpha} - \frac{m_{PL} g l cos(\alpha)}{2} \end{cases} \tag{6.15}$$

Chapter 7

Prototype's control

In this chapter the control of the quadrotor equipped with a robotic manipulator will be developed. The control that will be described is a Linear Quadratic Gaussian control, which involves an LQR controller and a Kalman Filter as the observer.

7.1 Introduction

The Quadrotor system equipped with a robotic manipulator is an unstable system and therefore it is necessary to design a controller that is capable of controlling and stabilizing it. There are few works in the literature that deal with this purpose. One of the methods consists in using adaptive control [24], [27], and [57]. In all of the aforementioned works, two control loops are designed, one for the position and the other for the attitude. Moreover, the authors of [57] contemplate the manipulator and the quadrotor as two different systems, hence, the robotic arm is controlled with a PID. By contrast, in [55] the manipulator is added to the UAV, which influences the global inertia and mass. In this case, a double integrator system is employed for stabilizing both the vehicle and the arm. Finally, two alternative methods are discussed in [58]. One of them consists in a combination of various PID controllers, located in a cascade form. The other implementation is a backstepping integral controller, in which the manipulator is contemplated as a perturbation and two loops are needed.

The current project proposes an innovative control in which an LQG regulator is used for the quadrotor's control while the manipulator uses a PID one. Both methods require the system equation's linearization. Thus, an overview of the procedure and methods used will be done hereafter. For a better understanding of the algorithm, a block diagram of the control proposal, supposing that all the variables are known, is attached below.

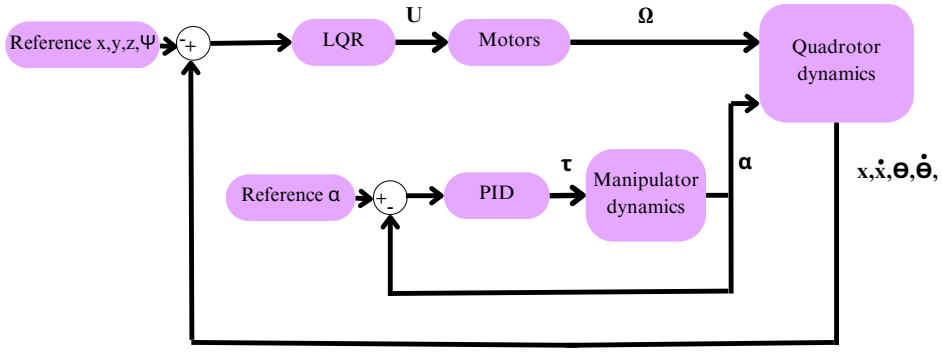

Figure 7.1: LQR and PID control block diagram

However, in reality, the position and altitude derivatives $(\dot{x}, \dot{y}, \dot{z})$ are not measured directly by the sensors. Hence, these variables should be estimated, and to do so the Kalman filter is implemented. The combination of an LQR controller and the Kalman filter as a state estimator is named LQG. The block diagram then is as follows:

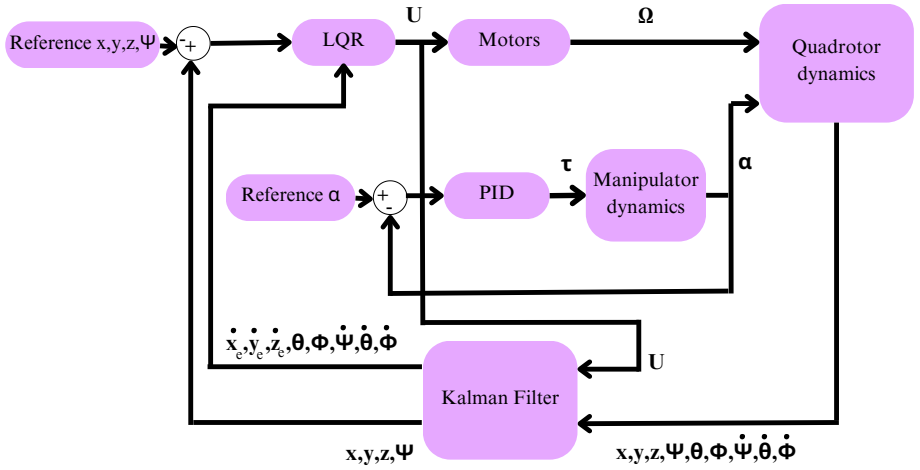

Figure 7.2: LQG and PID control block diagram

Where the subindex e denotes they are estimated values.

7.1.1 Linealization

Since controlling non-linear models is complex, the first step is to linearize the expressions of the model using Taylor series. All the linearizations are made around a selected point of reference (x_0, u_0). The first step is to set all the parameters that will be studied in the state space form, meaning all the variables and their derivatives are renamed as x_i. In fact, the variables are given an x_i in which i corresponds to an odd number, while their derivatives are x_{i+1}. Once this change is applied and the model is represented in the canonical form, the desired equation is:

$$\begin{cases} \dot{\overline{x}} = A\overline{x} + B\overline{u} \\ \overline{y} = C\overline{x} + D\overline{u} \end{cases} \tag{7.1}$$

Where the overlined parameters represent the difference between the actual parameter and the operating point.

$$\overline{x} = x - x_0 \qquad \overline{u} = u - u_0$$

While the upper expression corresponds to the linearized state equation, the lower is the measured states one. **A,B,C**, and **D** are Jacobian matrices that could be determined as:

$$A = \begin{bmatrix} \frac{\delta f_1}{\delta x_1} & \cdots & \frac{\delta f_1}{\delta x_n} \\ \vdots & \ddots & \vdots \\ \frac{\delta f_n}{\delta x_1} & \cdots & \frac{\delta f_n}{\delta x_n} \end{bmatrix}_{OP} \qquad B = \begin{bmatrix} \frac{\delta f_1}{\delta u_1} & \cdots & \frac{\delta f_1}{\delta u_n} \\ \vdots & \ddots & \vdots \\ \frac{\delta f_n}{\delta u_1} & \cdots & \frac{\delta f_n}{\delta u_n} \end{bmatrix}_{OP}$$

$$C = \begin{bmatrix} \frac{\delta h_1}{\delta x_1} & \cdots & \frac{\delta h_1}{\delta x_n} \\ \vdots & \ddots & \vdots \\ \frac{\delta h_n}{\delta x_1} & \cdots & \frac{\delta h_n}{\delta x_n} \end{bmatrix}_{OP} \qquad D = \begin{bmatrix} \frac{\delta h_1}{\delta u_1} & \cdots & \frac{\delta h_1}{\delta u_n} \\ \vdots & \ddots & \vdots \\ \frac{\delta h_n}{\delta u_1} & \cdots & \frac{\delta h_n}{\delta u_n} \end{bmatrix}_{OP}$$

Where OP means evaluated in the Operating Point. Finally, by evaluating the matrices in the operating point, the linearization of the system is accomplished.

7.1.2 Proportional integral derivative controller

Proportional Integrative Derivative (PID) is a well kown and most popular controller which tries to bring the error, difference between the reference signal and the measured value, $e(t) = x_{ref} - x$, to zero. The linearized state equation is attached below.

$$u(t) = K_P e(t) + K_I \int_0^t e(t)dt + K_D \frac{de(t)}{dt}$$

The numerical values of the constants are used for adjusting the performance of the controller and each of them influences $u(t)$ in a different way. The proportional control ($K_P e(t)$) is directly related to the error, meaning that if the error is high, the correction will be too. Regarding the integral part ($K_I \int_0^t e(t)\delta t$), it helps readjusting $u(t)$ by taking into account the accumulative error. Furthermore, it also improves the response's stability. Finally, a derivative control ($K_D \frac{\delta e(t)}{\delta t}$) can dampen oscillations and improve stability, but it can also amplify the effect of noise. It changes $u(t)$ considering the rate of changes produced in the error [59].

7.1.3 Linear Quadratic Gaussian Control (LQG)

The Linear Quadratic Gaussian Control is a state-feedback control that uses LQR as the controller and Kalman Filter as the observer.

Linear Quadratic Regulator

The linear quadratic regulator (LQR) is a feedback controller, which procedure consists in the optimization of a function named *cost function* [60, 61]. Taking, for instance, the following linear system:

$$\begin{cases} \dot{x}(t) = Ax(t) + Bu(t) \\ \dot{y}(t) = Cx(t) + Du(t) \end{cases}$$

Where **x** is the state vector and **u** is the control input and $x(t_0) = x_0$.

The quadratic cost function that needs to be minimized is:

$$C = \frac{1}{2}\int_{t_0}^{t_f} \left[y^T(t)Qy(t) + u^T(t)Ru(t)\right] dt + \frac{1}{2}x^T(t_f)P_{t_f}x(t_f)$$

The matrices **Q** and **R** are diagonal positive defined design matrices that are variated in order to improve the control. They are also named design functions.

Having defined the cost function and considering a linear controller, the optimum input can be accomplished taking:

$$u(t) = -K(t)x(t)$$

Meaning that the appropriate **K** should be computed. This new parameter can be calculated by solving the Riccati equation, since:

$$K = R^{-1}B^T P$$

Where **P** is the positive-definite matrix solution of the Riccati equation attached below.

$$-\dot{P}(t) = AP(t) + P(t)A + C^T QC - P(t)BR^{-1}B^T P(t)$$

Once the optimal **K** is established, it is added as a gain in the control loop. The determination of the matrix can be obtained by using the *MATLAB* already developed function *lqr()* of the control toolbox.

Kalman Filter

The Kalman filter is used as a state estimator in the *LQG*. The estimator is an essential component of the control of a quadrotor because there are some measurements that the sensors cannot acquire, such as the position and altitude derivatives. Kalman Filter permits estimating a state (x) through a known measurement

(z_k) [62].

$$x_k = Ax_{k-1} + Bu_{k-1} + w_{k-1}$$
$$z_k = Hx_k + v_k$$

Where w_k is the process noise, which has a process noise covariance $\mathbf{Q}$, and v_k is the measurement noise, which has a measurement noise covariance $\mathbf{R}$. Generally, they are assumed white, with normal probability distributions, and independent one from another.

The process can be divided into two distinct subsequent procedures, time update or prediction (the state is estimated) and measurement update or correction (the estimation is corrected). Starting with the latter, some initial estimates of $\hat{x}_{k-1}$ and P_{k-1} are established. Then the next state and covariance are predicted with the expressions:

$$\hat{x}_k^- = A\hat{x}_{k-1} + Bu_{k-1}$$
$$P_k^- = AP_{k-1}A^T + Q$$

Where P_k corresponds to the error covariance. Then, a measurement is acquired and the correction is made using the predicted x_k^- and P_k^- the equations expressed below.

$$K_k = P_k^- H^T (HP_k^- H^T + R)^{-1}$$
$$\hat{x_k} = \hat{x_k}^- + K_k(z_k - H\hat{x_k^-})$$
$$P_k = (I - K_k H)P_k^-$$

K_k is the Kalman gain and the computed P_k and $\hat{x_k}$ are introduced again in the time update equations and a loop is created. The value of the Kalman gain can be obtained through the function *lqe()* of *MATLAB/SIMULINK*.

The main benefit of using the Kalman filter is that not only is the estimation achieved but noise can also be filtered.

7.2 Nonlinear simulation

Before making any consideration about the prototype's control, the mathematical models defined in Equations (6.7) and (6.10) should be implemented in *MATLAB/SIMULINK* for validating their response.

There are some variables from both the quadrotor and the manipulator, whose values are required for the simulation process, such as the quadrotor's weight or its inertia. The following Table includes all of them with their respective numerical values.

Simulation parameters	
m [kg]	6.3
l [m]	0.453
I_{xx}[kg·m^2]	0.246
I_{yy}[kg·m^2]	0.246
I_{zz}[kg·m^2]	0.401
g [m/s^2]	9.8
J_r[kg·m^2]	$8.66{\cdot}10^{-7}$
b[N·s^2]	$3.5{*}10{\cdot}10^{-5}$
d[N·$m \cdot s^2$]	$7.42{*}10{\cdot}10^{-7}$
Ω_{max}[rad/s]	800
m_{pl} [kg]	1
l_m[m]	0.32
I_{ym}[kg·m^2]	0.0341

Table 7.1: Parameters indispensable for the simulations

The ones that were not computed in any previous section of the report ate extracted from similar quadrotors in the literature [63].

7.2.1 Nonlinear quadrotor

Firstly, Equation (6.7) is implemented in *MATLAB/SIMULINK*, and the quadrotor performance is examined by giving certain values to the rotors' velocities. The first response studied is the hover position, meaning all the rotors are given the same velocity, which should be high enough to enable the UAV's climb. The graphics obtained from the simulation are attached below.

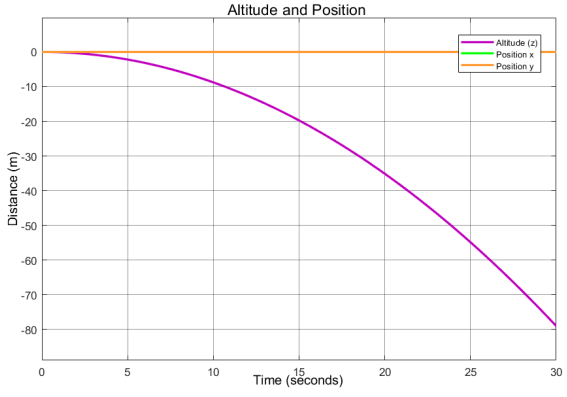

(a) Altitude and position response.

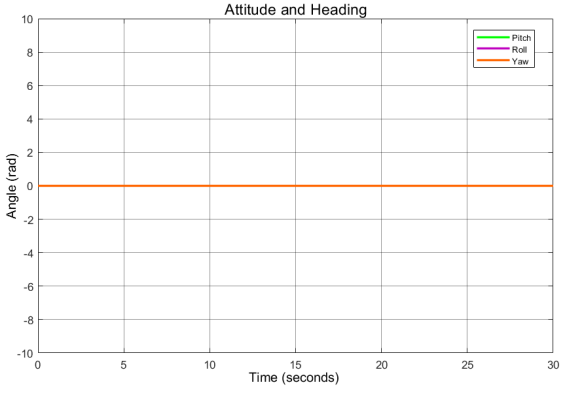

(b) Attitude response.

Figure 7.3: Hover response.

Since there is no variation in the attitude and the only parameter that varies is the altitude, the hover response is, hence, validated. Hereafter, a positive roll is intended by increasing the speed of rotor number

4 while decreasing the number 2. The rotor's numeration can be observed in Figure 6.1. The altitude and position as well as the attitude response are portrayed in the following Figure.

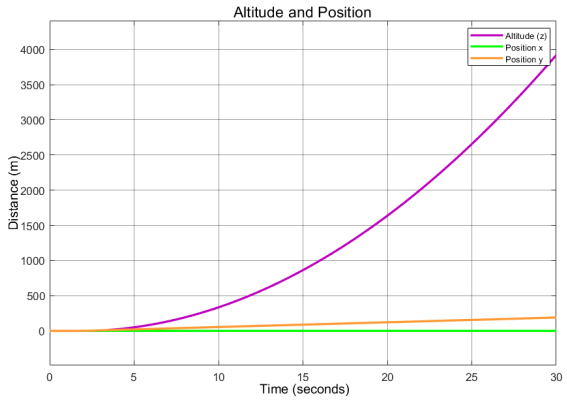

(a) Altitude and position response.

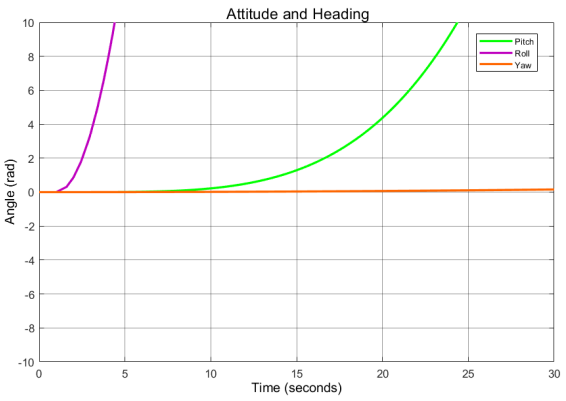

(b) Attitude response.

Figure 7.4: Roll response.

As it was expected, a positive roll is generated and it slightly induces a movement in the pitch angle. When it comes to the altitude and position simulation, roll produces a positive variation in the y-direction while the drone is expected to reduce its height. Meaning that the effect of the roll is properly simulated.

In order to validate the pitch movement, rotor number 1 is speeded up and rotor 4 is slowed down simultaneously. Hence, a positive pitch is expected. The effects on altitude, position, and attitude are plotted and attached below.

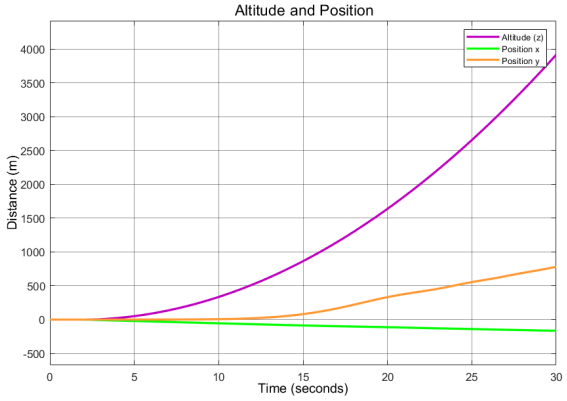

(a) Altitude and position response.

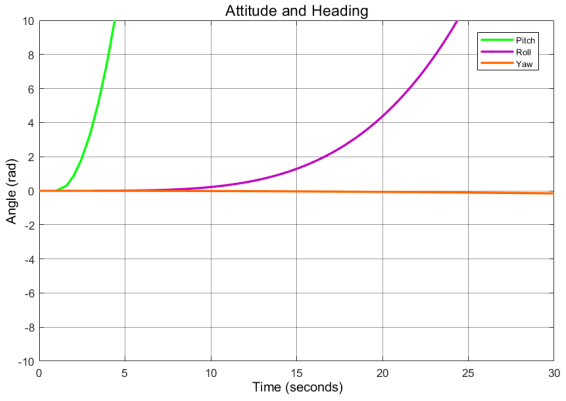

(b) Attitude response.

Figure 7.5: Pitch response.

The desired positive pitch is achieved and it slightly influences the roll angle. Once again, validating the coupling between the two angles. In fact, the little deviation of the y-position is also originated because of it. A negative variation in the x-position and the descent of the quadrotor were also anticipated.

Finally, by speeding up rotors 2 and 4 while slowing down rotors 1 and 3, a positive yaw is expected. The simulation response in terms of altitude and position and attitude is plotted and attached in the following Figure.

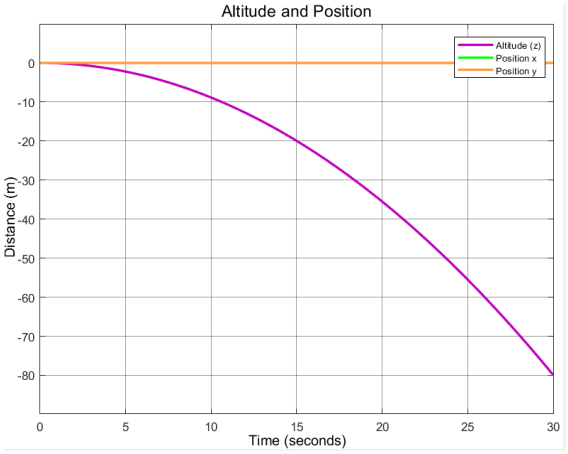

(a) Altitude and position response.

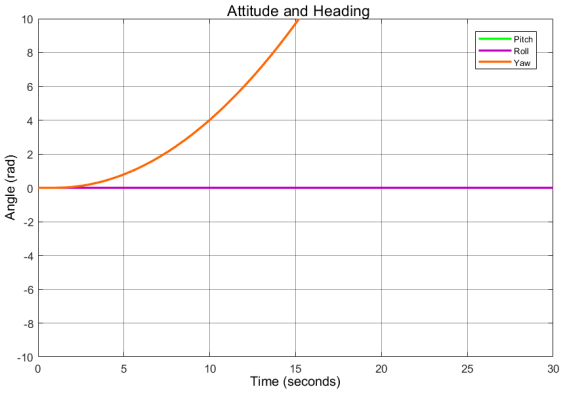

(b) Attitude response.

Figure 7.6: Yaw response.

The effects achieved are a positive pitch, as was desired, and a negative attitude, meaning the drone is climbing. There is no change in any of the other variables, which ensures the proper response of the yaw movement.

7.2.2 Quadrotor with robotic arm nonlinear model

Having verified the nonlinear system of the quadrotor, the effects of the arm can be added so as to simulate the behavior of the UAV when it is equipped with the manipulator. Therefore, Equation (6.15) is introduced in *MATLAB/SIMULINK* and a value of $\alpha = \frac{-\pi}{2}$ is settled. The latter corresponds to the position of the arm that is supposed to influence the UAV the least. In the same way as it was done in the previous Section, the four rotors are given the same speed in order to acquire the hover response, which results as the following Figure portrays.

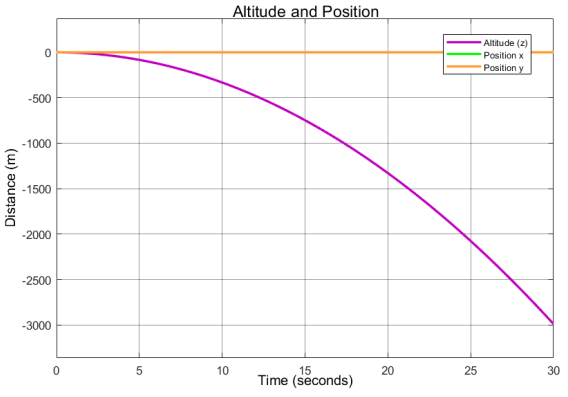

(a) Altitude and position response.

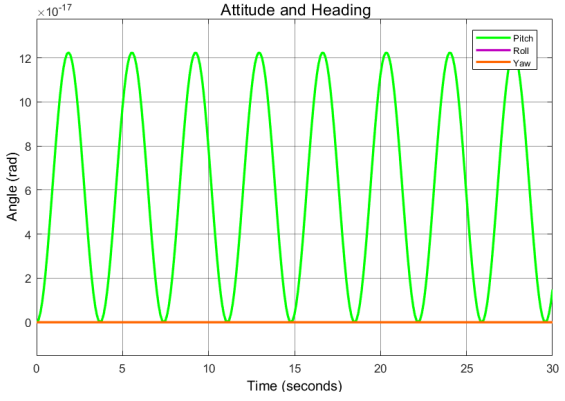

(b) Attitude response.

Figure 7.7: Model hover response.

While the altitude and position of the vehicle resemble the scenario where there is no manipulator, there are some small variations in the pitch angle that were not in the previous model. However, the magnitude of such oscillation is so little that it can be neglected.

The next response to simulate, the roll movement, is achieved by speeding up rotor 4 and decreasing the speed of rotor 2. In the Figure attached below the altitude, position, and attitude behavior of the drone are plotted.

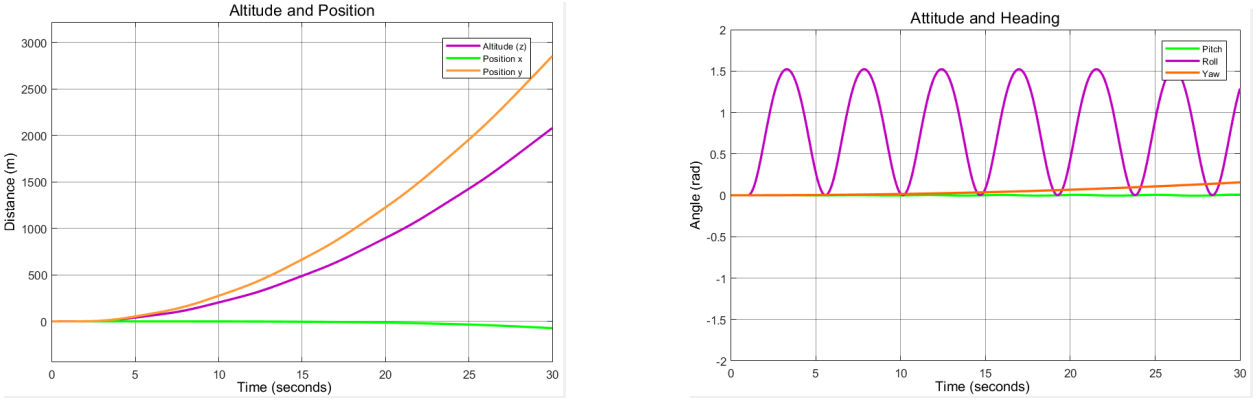

(a) Altitude and position response.

(b) Attitude response.

Figure 7.8: Model roll response.

In this case, the presence of the manipulator produces oscillations around the x-axis of the drone, meaning the roll oscillates. Regarding the rest of the studied variables, their response is the same as when there was no robotic arm.

Hereafter, the speed of rotor number 1 is increased while, simultaneously, rotor number 3 is slowed down. The simulation behavior regarding altitude, position, and attitude is plotted in the following graphics:

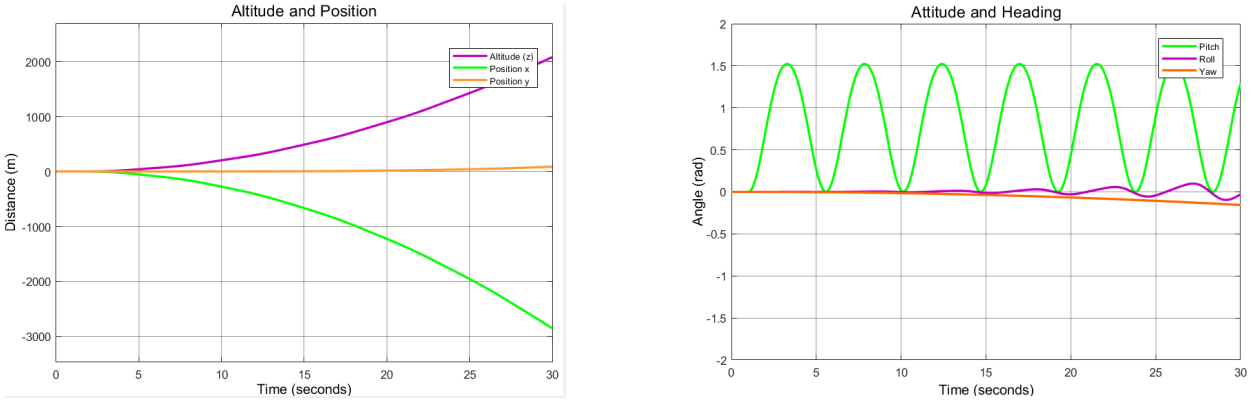

(a) Altitude and position response.

(b) Attitude response.

Figure 7.9: Model pitch response.

Not only is the pitch affected by the manipulators but also the roll, although the latter oscillates far less. The response in the position is the same one as when the quadrotor was not carrying the arm.

Finally, the yaw response of the system is plotted by speeding up rotors number 2 and 4, while the other two are slowed down.

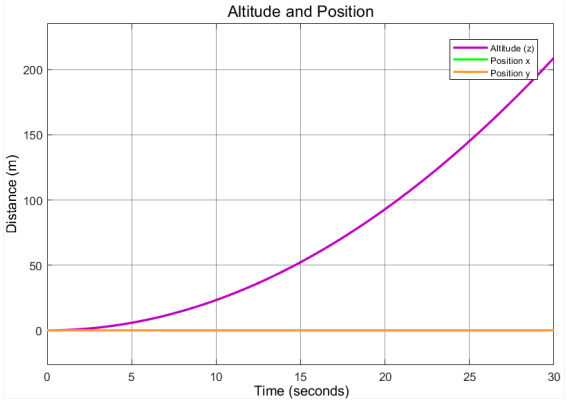

(a) Altitude and position response.

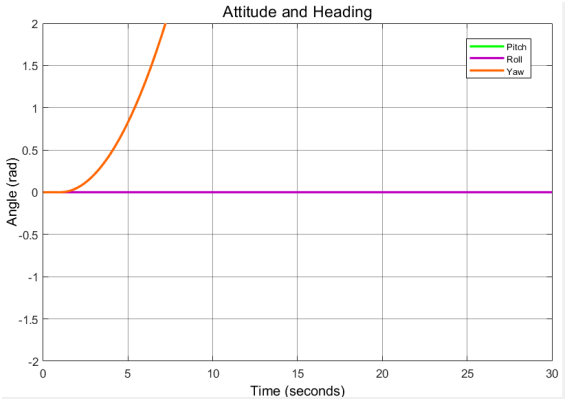

(b) Attitude response.

Figure 7.10: Model yaw response.

As the Figure below shows, the effect of changing the yaw angle is not influenced by the manipulator. The response in terms of attitude is the same as if there was no payload. When it comes to the altitude, however, the UAV is descending, since more thrust is required as more weight has to be lifted.

7.3 Quadrotor's control

Once the behavior of both nonlinear models is verified, the actual control of the quadrotor can be carried out. First and foremost, the control of only the quadrotor, without the manipulator attached to it, is computed. In this section the linearization of the UAV's model and its control using LQG are conducted contemplating Section 5.1.

7.3.1 Quadrotor's linearization

As it was detailed in the intoduction of Section 7.1, the linearization of Equation (6.7) should be done. To do so, the change of variables selected is as follows:

$$x_1 = \phi \quad x_2 = \dot{x_1} = p \quad x_3 = \theta \quad x_4 = \dot{x_3} = q \quad x_5 = \psi \quad x_6 = \dot{x_5} = r$$

$$x_7 = \dot{z} \quad x_8 = \dot{x_7} = \ddot{z} \quad x_9 = \dot{x} \quad x_{10} = \dot{x_9} = \ddot{x} \quad x_{11} = \dot{y} \quad x_{12} = \dot{x_{11}} = \ddot{y}$$

Resulting in the following canonical state space form:

$$\begin{bmatrix} \dot{x_1} \\ \dot{x_2} \\ \dot{x_3} \\ \dot{x_4} \\ \dot{x_5} \\ \dot{x_6} \\ \dot{x_7} \\ \dot{x_8} \\ \dot{x_9} \\ \dot{x_{10}} \\ \dot{x_{11}} \\ \dot{x_{12}} \end{bmatrix} = \begin{bmatrix} x_2 \\ \frac{I_{yy}-I_{zz}}{I_{xx}} x_4 x_6 - \frac{J_p \Omega_r}{I_{xx}} x_4 + \frac{U_2}{I_{xx}} \\ x_4 \\ \frac{I_{zz}-I_{xx}}{I_{yy}} x_2 x_6 - \frac{J_p \Omega_r}{I_{yy}} x_2 + \frac{U_3}{I_{yy}} \\ x_6 \\ \frac{I_{xx}-I_{yy}}{I_{zz}} x_2 x_4 + \frac{U_4}{I_{zz}} \\ x_8 \\ -cos(x_1)cos(x_3)\frac{U_1}{m_T} + g \\ x_{10} \\ -(cos(x_1)sin(x_3)cos(x_5) + sin(x_1)sin(x_5))\frac{U_1}{m_T} \\ x_{12} \\ -(cos(x_1)sin(x_3)sin(x_5) - sin(x_3)cos(x_5))\frac{U_1}{m_T} \end{bmatrix}$$

Thereafter, for computing the values of the matrices **A,B,C**, and **D**, the *MATLAB* function *Jacobian* is used. The latter is capable of computing the Jacobian matrix of a function regarding the specified variables. The reference point should also be defined, subsequently, the hover position is selected, and the values given to the parameters, both the state space and the inputs, are:

$$x_1 = 0 \quad x_2 = 0 = p \quad x_3 = 0 \quad x_4 = 0 \quad x_5 = 0 \quad x_6 = 0$$

$$x_7 = -1 \quad x_8 = 0 \quad x_90 \quad x_{10} = 0 \quad x_{11} = 0 \quad x_{12} = 0$$

$$u_1 = m \cdot g \quad u_2 = 0 \quad u_3 = 0 \quad u_4 = 0$$

Substituting this values in the Jacobian matrices computed by *MATLAB*, the matrices **A,B,C**, and **D** result:

$$A = \begin{bmatrix} 0 & 1 & 0 & 0 & 0 & 0 & 0 & 0 & 0 & 0 & 0 & 0 \\ 0 & 0 & 0 & 0 & 0 & 0 & 0 & 0 & 0 & 0 & 0 & 0 \\ 0 & 0 & 0 & 1 & 0 & 0 & 0 & 0 & 0 & 0 & 0 & 0 \\ 0 & 0 & 0 & 0 & 0 & 0 & 0 & 0 & 0 & 0 & 0 & 0 \\ 0 & 0 & 0 & 0 & 0 & 1 & 0 & 0 & 0 & 0 & 0 & 0 \\ 0 & 0 & 0 & 0 & 0 & 0 & 0 & 0 & 0 & 0 & 0 & 0 \\ 0 & 0 & 0 & 0 & 0 & 0 & 0 & 1 & 0 & 0 & 0 & 0 \\ 0 & 0 & 0 & 0 & 0 & 0 & 0 & 0 & 0 & 0 & 0 & 0 \\ 0 & 0 & 0 & 0 & 0 & 0 & 0 & 0 & 0 & 1 & 0 & 0 \\ 0 & 0 & -9.8 & 0 & 0 & 0 & 0 & 0 & 0 & 0 & 0 & 0 \\ 0 & 0 & 0 & 0 & 0 & 0 & 0 & 0 & 0 & 0 & 0 & 1 \\ -9.8 & 0 & 0 & 0 & 0 & 0 & 0 & 0 & 0 & 0 & 0 & 0 \end{bmatrix} \qquad B = \begin{bmatrix} 0 & 0 & 0 & 0 \\ 0 & 1.842 & 0 & 0 \\ 0 & 0 & 0 & 0 \\ 0 & 0 & 1.842 & 0 \\ 0 & 0 & 0 & 0 \\ 0 & 0 & 0 & 2.494 \\ 0 & 0 & 0 & 0 \\ -0.159 & 0 & 0 & 0 \\ 0 & 0 & 0 & 0 \\ 0 & 0 & 0 & 0 \\ 0 & 0 & 0 & 0 \\ 0 & 0 & 0 & 0 \end{bmatrix}$$

$$C = I_{12\times 12} \qquad D = 0_{12\times 4}$$

All the obtained results are saved in a *MATLAB* code so as to perform the control.

7.3.2 Quadrotor's LQG regulator

Having the system linearized, the design of the LQG starts with the LQR determination. For this purpose, another *MATLAB* function capable of computing the optimal gain (K) for the model is used. This function has four inputs, two of which are the matrices **A** and **B** determined in the linearization. The remaining two correspond to the design matrices **Q** and **R** characteristic of the LQR controller. The function in the code is written as follows:

$$K = lqr(A, B, Q, R)$$

For selecting the best **R** and **Q** matrices, the reference control values have to be established. Being a multivariable system, not all the parameters of the quadrotor can be simultaneously adjusted. The factors that are adjusted will be the position in x, the position in y, the altitude, and the movement in the yaw angle. The values of such will be:

$$ref = \begin{bmatrix} x_{ref} & y_{ref} & z_{ref} & \psi_{ref} \end{bmatrix}' = \begin{bmatrix} 1 & 1 & 1 & 0.2 \end{bmatrix}'$$

After some trial and error, the configurations of **R** and **Q** which response was better are:

$$R = diag\begin{pmatrix} 1 & 1 & 1 & 1 \end{pmatrix}$$

$$Q = diag\begin{pmatrix} 1 & 1 & 1 & 1 & 1 & 1 & 0.5 & 1 & 0.5 & 1 & 0.5 & 1 \end{pmatrix}$$

Having designed the LQR controller, the observer (Kalman filter) can be drawn up too. Since it has filtering properties, as its name says, Gaussian noise is added with the features shown in the next Figure.

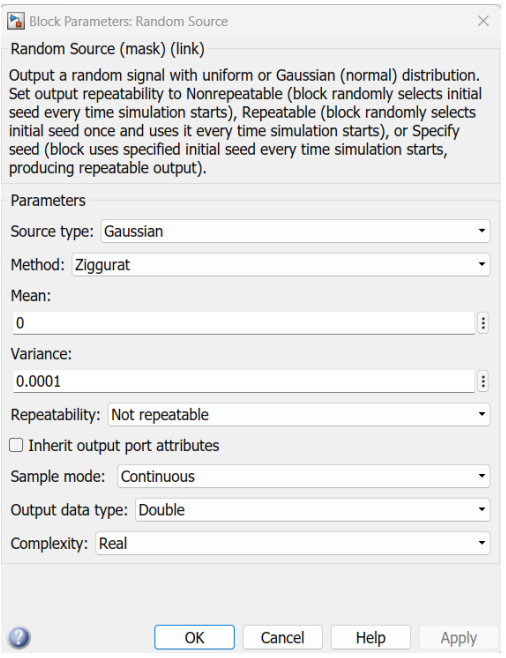

Figure 7.11: Noise conditions

The *MATLAB/SIMULINK* function used for determining the Kalman gain (K_e) is added in the code as:

$$Ke = lqe(A, G, C, QQ, RR, NN)$$

Where **A** is the linearization jacobian matrix, and **G** is the matrice that multiplies the process noise. Since all the parameters are affected by the process noise, **G** is $I_{12\times12}$. **C** is the linearization Jacobian matrix but only considering the known states, which are all of them except for the position and altitude derivatives ($\dot{x}, \dot{y}$, and $\dot{y}$). Matrices **QQ** and **RR** are respectively the process and the measurement noise covariances, and **NN** is the noise cross-covariance. The values established for the matrices **C**, **QQ**, **RR**, and **NN** are:

$$QQ = 0.0001 \cdot I_{12\times12} \qquad RR = 0.0001 \cdot I_{9\times9} \qquad NN = 0_{12\times9}$$

$$C = \begin{bmatrix} 1 & 0 & 0 & 0 & 0 & 0 & 0 & 0 & 0 & 0 & 0 & 0 \\ 0 & 1 & 0 & 0 & 0 & 0 & 0 & 0 & 0 & 0 & 0 & 0 \\ 0 & 0 & 1 & 0 & 0 & 0 & 0 & 0 & 0 & 0 & 0 & 0 \\ 0 & 0 & 0 & 1 & 0 & 0 & 0 & 0 & 0 & 0 & 0 & 0 \\ 0 & 0 & 0 & 0 & 1 & 0 & 0 & 0 & 0 & 0 & 0 & 0 \\ 0 & 0 & 0 & 0 & 0 & 1 & 0 & 0 & 0 & 0 & 0 & 0 \\ 0 & 0 & 0 & 0 & 0 & 0 & 1 & 0 & 0 & 0 & 0 & 0 \\ 0 & 0 & 0 & 0 & 0 & 0 & 0 & 0 & 1 & 0 & 0 & 0 \\ 0 & 0 & 0 & 0 & 0 & 0 & 0 & 0 & 0 & 0 & 1 & 0 \end{bmatrix} \tag{7.2}$$

Finally, the system response can be analyzed. Despite having some small oscillations, position x and position y get to the reference value and can be supposed as stable. Moreover, both factors have a rapid response, they arrive at the reference in less than 8 *seconds*. When it comes to the altitude, it is the latest in reaching the reference value (20 *seconds*) but once it is achieved the system becomes stable. The tardiness of the altitude is justified since the obtained response has the smallest overshoot. Last but not least, the yaw response is the best one since not only does it get rapidly to the reference point (5 *seconds*) but it also becomes stable. A rapid response is also ensured. Therefore, the whole system is considered as steady and controlled. These outcomes can be observed in the next Figure.

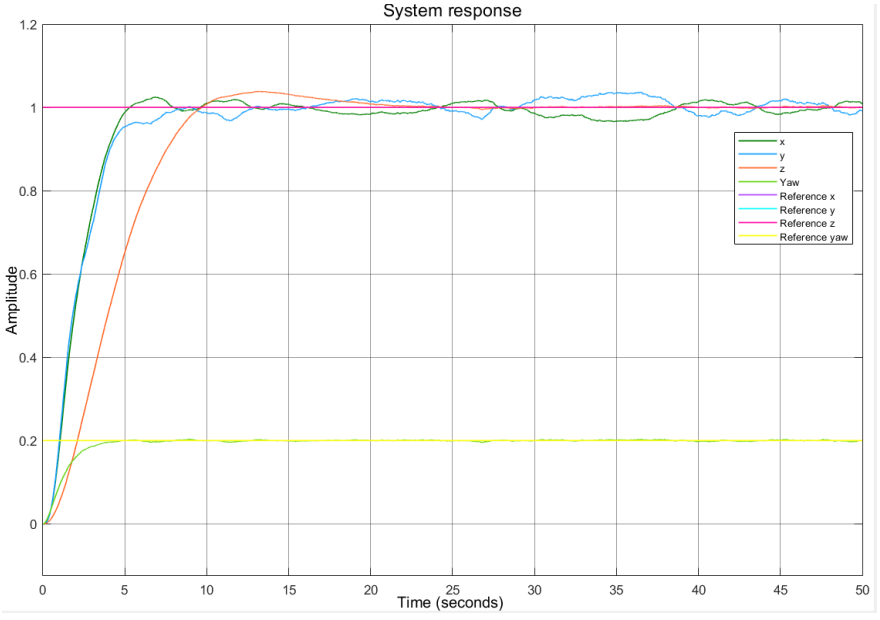

Figure 7.12: LQG control applied to the quadrotor.

For ensuring the correct operation of the filter, the response of the system before Kalman but after the noise is applied is attached below.

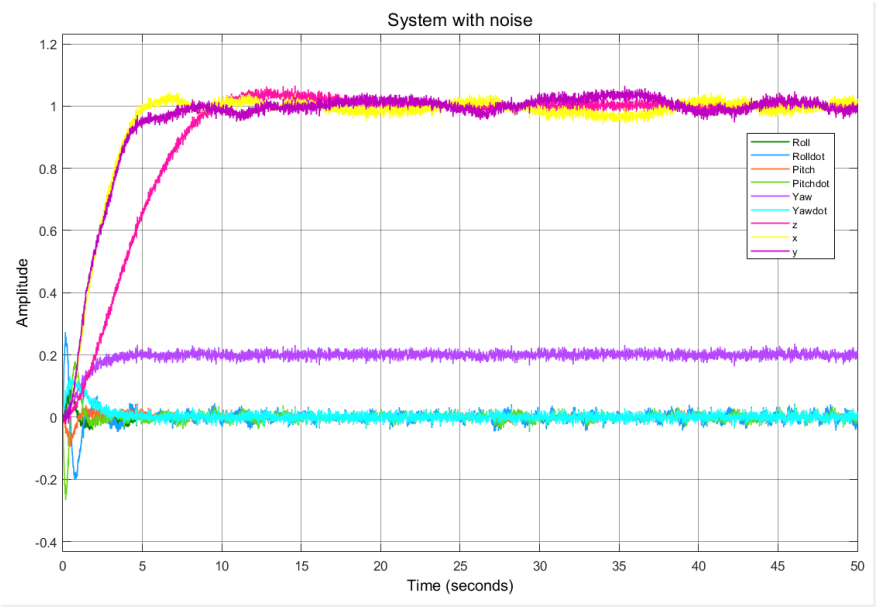

Figure 7.13: Response of the quadrotor with noise.

The difference between Figures 7.12 and 7.13 is considerable. All the oscillations produced by the noise added in the latter have been perfectly filtered by the Kalman Filter. Hence, the observer performance is validated in terms of filtering as well as of estimating.

7.4 Prototype's control

The control of the prototype involves not only the quadrotor's control but also the manipulator's one. This section will be divided into three subsections: the design of the controls, the response when the arm is fixed, and the response when the cleaning is being done.

7.4.1 Manipulator and quadrotor control

Quadrotor

Starting with the UAV's control, the same procedure stated in the previous Section 7.3 is followed. However, since the global weight is increased, it affects the equilibrium point taken as a reference in the linearization. The new reference point considered is:

$$x_1 = 0 \quad x_2 = 0 = p \quad x_3 = 0 \quad x_4 = 0 \quad x_5 = 0 \quad x_6 = 0$$

$$x_7 = -1 \quad x_8 = 0 \quad x_90 \quad x_{10} = 0 \quad x_{11} = 0 \quad x_{12} = 0$$

$$u_1 = (m + m_{PL}) \cdot g \quad u_2 = 0 \quad u_3 = 0 \quad u_4 = 0$$

This change affects the linear matrices **A** and **B**, giving now the following values.

$$A = \begin{bmatrix} 0 & 1 & 0 & 0 & 0 & 0 & 0 & 0 & 0 & 0 & 0 & 0 \\ 0 & 0 & 0 & 0 & 0 & 0 & 0 & 0 & 0 & 0 & 0 & 0 \\ 0 & 0 & 0 & 1 & 0 & 0 & 0 & 0 & 0 & 0 & 0 & 0 \\ 0 & 0 & 0 & 0 & 0 & 0 & 0 & 0 & 0 & 0 & 0 & 0 \\ 0 & 0 & 0 & 0 & 0 & 1 & 0 & 0 & 0 & 0 & 0 & 0 \\ 0 & 0 & 0 & 0 & 0 & 0 & 0 & 0 & 0 & 0 & 0 & 0 \\ 0 & 0 & 0 & 0 & 0 & 0 & 0 & 1 & 0 & 0 & 0 & 0 \\ 0 & 0 & 0 & 0 & 0 & 0 & 0 & 0 & 0 & 0 & 0 & 0 \\ 0 & 0 & 0 & 0 & 0 & 0 & 0 & 0 & 0 & 1 & 0 & 0 \\ 0 & 0 & -11.356 & 0 & 0 & 0 & 0 & 0 & 0 & 0 & 0 & 0 \\ 0 & 0 & 0 & 0 & 0 & 0 & 0 & 0 & 0 & 0 & 0 & 1 \\ 11.356 & 0 & 0 & 0 & 0 & 0 & 0 & 0 & 0 & 0 & 0 & 0 \end{bmatrix} \quad B = \begin{bmatrix} 0 & 0 & 0 & 0 \\ 0 & 1.842 & 0 & 0 \\ 0 & 0 & 0 & 0 \\ 0 & 0 & 1.842 & 0 \\ 0 & 0 & 0 & 0 \\ 0 & 0 & 0 & 2.494 \\ 0 & 0 & 0 & 0 \\ -0.159 & 0 & 0 & 0 \\ 0 & 0 & 0 & 0 \\ 0 & 0 & 0 & 0 \\ 0 & 0 & 0 & 0 \\ 0 & 0 & 0 & 0 \end{bmatrix}$$

Due to the previous matrices changes, the previously defined LQR design matrices **R** and **Q** do not provide a stable system. Once again, after trial and error, the design matrices whose response is adequate are:

$$R = diag \begin{pmatrix} 0.3 & 0.3 & 0.3 & 0.3 \end{pmatrix}$$

$$Q = diag \begin{pmatrix} 10 & 10 & 10 & 10 & 10 & 10 & 1000 & 10 & 1000 & 10 & 100 & 10 \end{pmatrix}$$

When it comes to the Kalman filter matrices and parameters, the same ones as in Section 7.3 are employed since the noise parameters have remained unchanged. The specified values of the noise are shown in Figure 7.11.

Manipulator

As it was mentioned in Section 7.1, a PID is applied for the manipulator. The fact that this control is based in the dynamics of the manipulator, which is expressed in Equation (6.13), needs to be emphasized. The constant values, which are presented in the Table below, were obtained after testing multiple combinations.

K_p	10
K_I	5
K_D	2

Table 7.2: PID manipulator constants.

Angle α is examined with two references, one being a fixed value and the other a sinus wave. The former corresponds to a value of $\frac{-\pi}{2}$, which is the manipulator's position when the cleaning task is not being developed. For computing an appropriate sinus wave, the difference between the maximum and minimum values that α can reach is taken as the amplitude. Moreover, a bias of -1.57 is set in order to ensure the limit angles are not surpassed. The following Figure represents the resulting sinus wave taken as a reference.

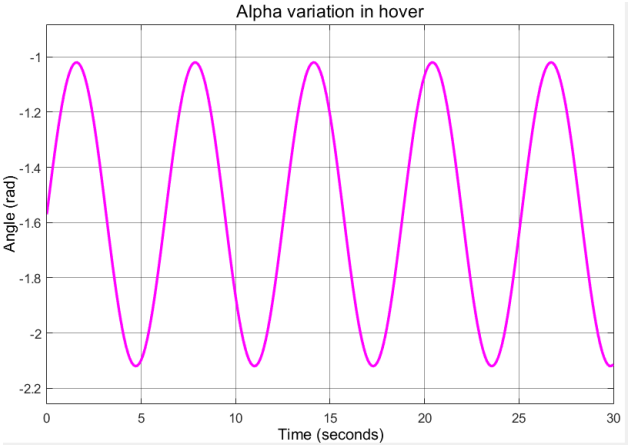

Figure 7.14: Sinus wave α plot.

Having defined the two scenarios the desired alpha could have, the PID is given the constants stated in Table 7.2 and the response results:

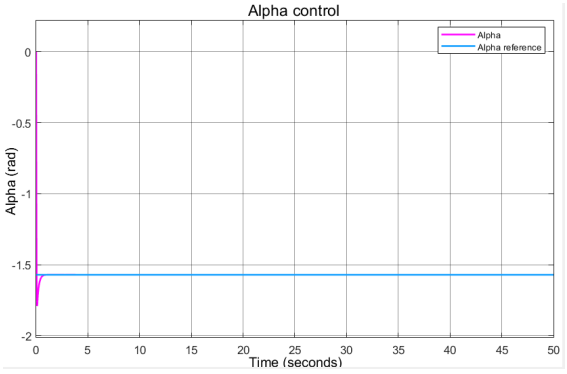

(a) Alpha control when its value is $\frac{-\pi}{2}$.

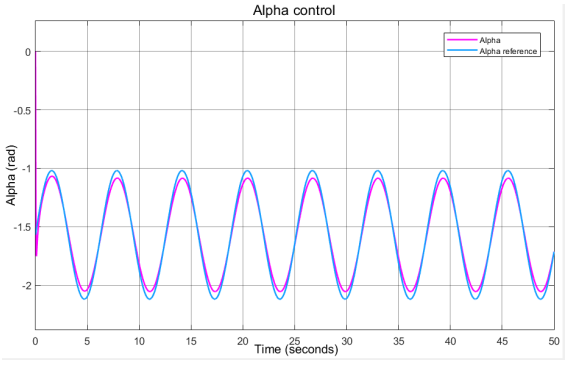

(b) Alpha control while cleaning.

Figure 7.15: Alpha control demonstration.

In both cases, the output resembles the given reference nearly instantaneously and once it is achieved the system becomes steady. It should be noted, however, the fact that before getting to the response there is an overshoot.

The combination of both control methods can be observed in the final *MATLAB/SIMULINK* implementation, attached below in order to demonstrate its similarity with the block diagram of Figure 7.2. Moreover, it gives a general overview of the whole system that has been developed.

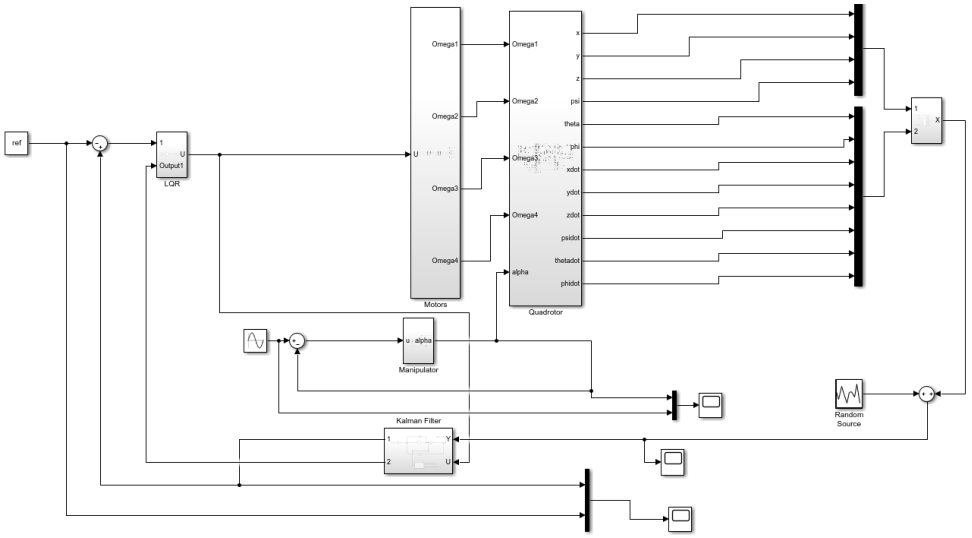

Figure 7.16: Simulink model.

7.4.2 Scenario 1: fixed manipulator

Taking the α control of Figure 7.15a, and the reference vector previously stated in Section 7.3.2, as well as all the defined matrices of the previous Section 7.4.1, the simulation plots the following response.

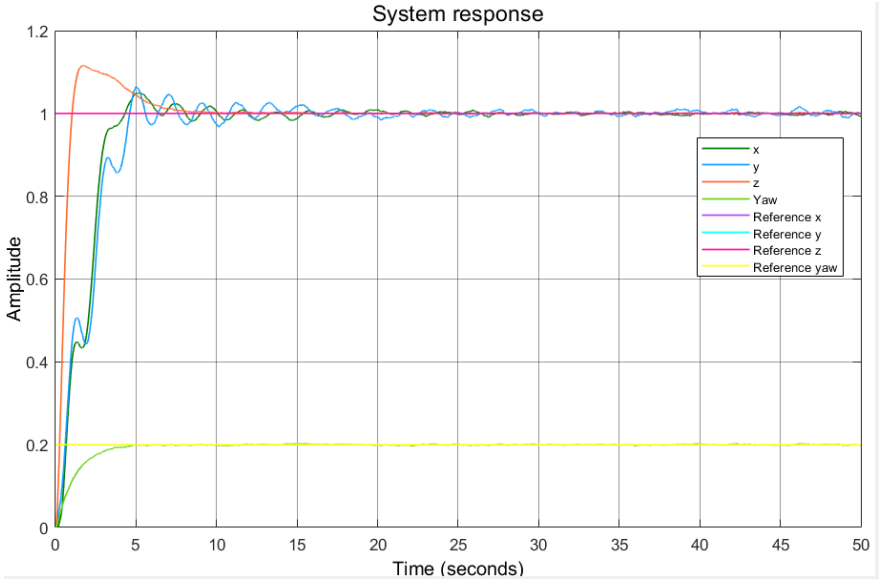

Figure 7.17: LQG control of the system.

In this scenario, the system response is not as smooth as in Figure 7.12. Nevertheless, the yaw response is quite similar, it becomes rapidly steady and to the reference point. When it comes to the positions of x and y, despite their oscillation, they reach the reference fairly quickly and their response becomes steadier with time.

Lastly, the altitude gets the reference value in a shorter time than in Figure 7.12 but with a higher overshoot.

Once again, for validating the performance of the state observer as a filter, the response with the noise is below attached.

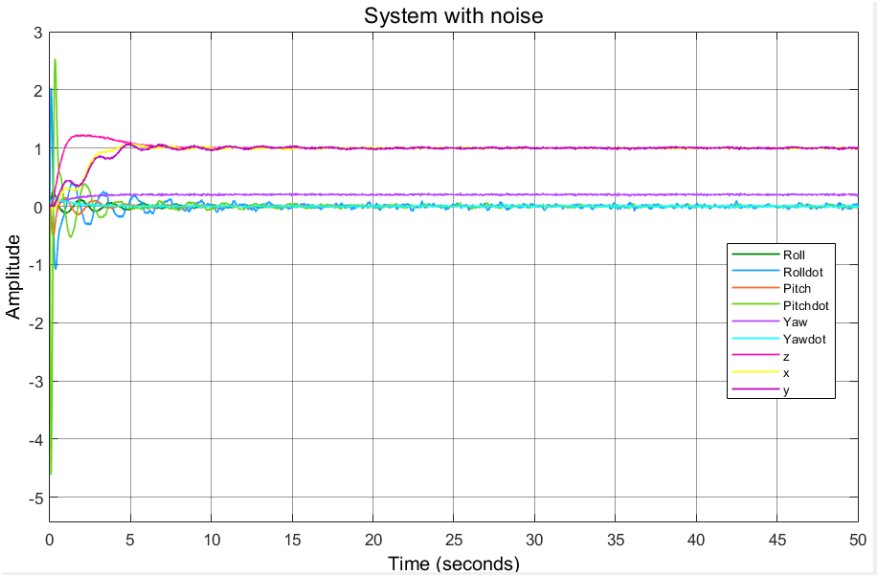

Figure 7.18: Response of the model with noise.

The difference between Figures 7.17 and 7.18 can be seen with the naked eye. All the random oscillations of the latter have disappeared in the former, validating, thus, the designed Kalman Filter.

7.4.3 Scenario 2: manipulator cleaning

The second studied case is when the angle α oscillates between its limits as portrayed in Figure 7.14. In this case, the noisy response of the model is not analyzed; the Kalman Filter is already validated. A simulation with the already established parameters and matrices is carried out, obtaining the following graphic.

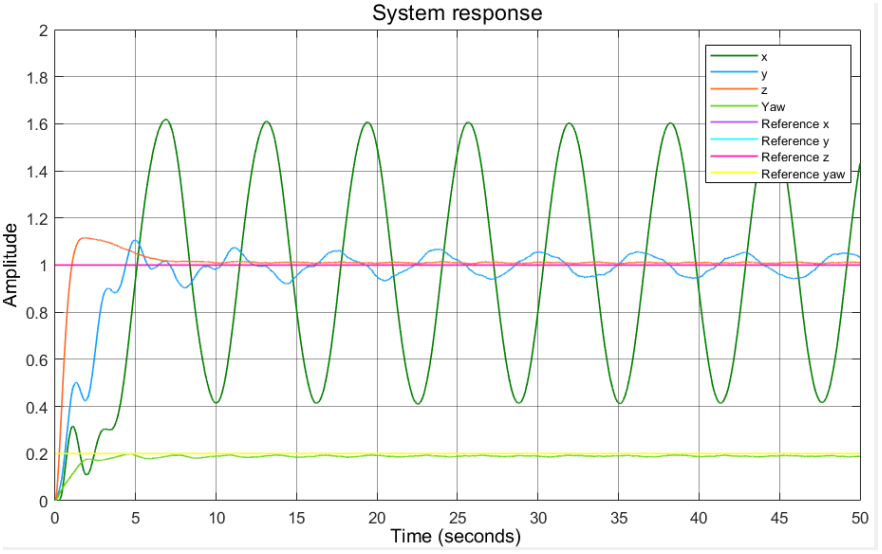

Figure 7.19: LQG control of the model.

From the graphic above the manipulator can be concluded to generate an oscillatory response to the positions x and y of the quadrotor. While the variations in the y position could be accepted, the x position changes do not represent a steady behavior. The altitude is not influenced by the payload's movement, thus, it still becomes rapidly steady with an initial overshoot. Finally, although it slightly oscillates, the yaw reaches the reference in a similar way as quickly as in the other scenarios.

As the previous model cannot be accepted, the angle variation allowed in α is reduced, being its maximum and minimum values $-1.47\ rad$ and $-1.67\ rad$. The alpha evolution and control of this modification is portrayed below.

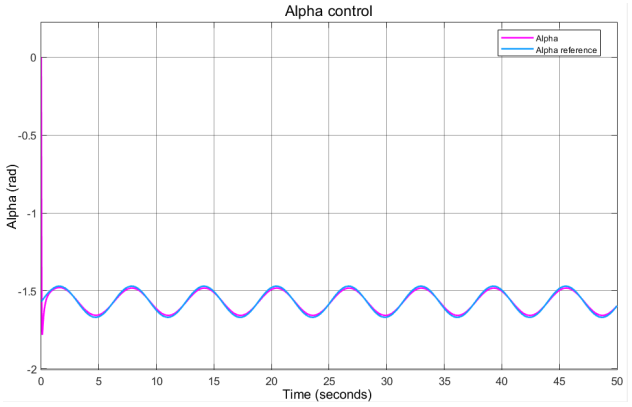

Figure 7.20: New modified α evolition.

The response of the system regarding this modification only varies from Figure 7.19 in terms of x and y positions. Their oscillation is reduced, being almost imperceptible in the y direction. The x value oscillates but with a lower amplitude, meaning it is not as steady as desired. However, this could be accepted since perfect control of the system can only be achieved when the manipulator is in $\alpha = \frac{-\pi}{2}$. Nevertheless, the fact that the quadrotor expression was linearized taking hovering as the reference point cannot be neglected. The latter implies that any variation from hovering will prevent the system from being steady. Therefore, the whole system is considered controlled when the α angle limitations are modified. The simulation graphic obtained in this case is as follows:

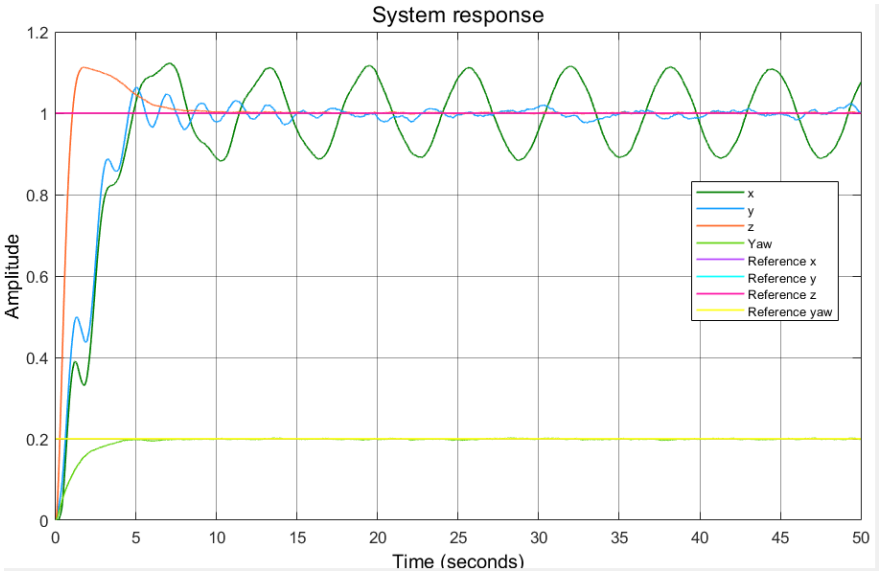

Figure 7.21: LQG control of the model.

Chapter 8

Environmental Impact

The current project can be divided into two distinct sections. The first one consists in the proposal's design and simulation, which is what has been developed in this report. The second part, however, is the experimental validation and future proposal implementation. The environmental impact of both will be examined below.

Regarding the design and simulation, there is minimal impact. All the procedure has been done using a laptop, meaning that all the footprint that it leaves is energy consumption. Assuming the employed laptop consumes 65 W, the estimated power needed is 21.84 kW. Taking the 2022 carbon footprint estimation of 259 $g\ CO_{2eq}/kWh$, the carbon footprint of the already developed study is 5.657 kg of CO_2 [64].

On the other hand, the proposal is to design an UAV capable of cleaning solar panels with the aim of easing this task. If the objective was achieved, it would be helpful for the boost of solar energy having an extremely positive environmental impact. Moreover, being a waterless and autonomous method, the only footprint it would leave is the one created by its components once they are no longer operative.

The most harmful components are the UAV's batteries which are made of Lithium Polymer (LiPo). Not only does lithium mining and the extraction required pollute but also does the recycling process needed for LiPo batteries. Moreover, more pollution is produced if such batteries malfunction due to defects or physical damage. Their proper maintenance is, therefore, imperative [65]. Even so, they tend to last over 300 to 500 cycles, which tends to be approximately 3 years. There are some manufacturers that bring up the possibility of a lifespan of 30 years if the maintenance is adequate [66]. In any event, the necessity of changing them is undeniable and it should be deeply analyzed before approving the implementation.

Chapter 9

Economic feasibility

In this chapter, the whole project budget will be summarized, the extended breakdown can be found in the document *"Study of an UAV implementation for solar panel cleaning-Budget"*. As it has been previously mentioned, the implementation project could be divided into the study (some of it being this report) and the experimental validation. The cost of both of them is analyzed.

In the budget document, the expenses of all the already-done work are detailed, giving a final amount of 4,100.08 €. This amount considers not only the software required but also the engineering hours of aerospace engineering at an internship level. Nevertheless, more simulations and a detailed design are remaining, which could increase the global study price up to over 10,121.85 €. In this case, the expenses are higher since the engineer in charge has already graduated.

Conversely, although the final prototype is not fully designed yet, an estimate of the product cost can be made with all the components that have been determined. The following Table summarizes the components and their prices.

Component	**Quantity**	**Price/Unit [€/u]**	**Total [€]**
Matrice 300 RTK	1	13,500.00 [31]	13,500.00
Manipulator	1	3,000 [67]	3,000
Mop structure	1	6.40 [28]	6.40
Microfiber cloth	50	10.10 [29]	50.50
	TOTAL		16,556.90

Table 9.1: First prototype budget estimation

It should be noted that the quantity of microfiber cloth is high since they are sold in that amount. Regarding the mop costs, a bigger mop's price has been set as an estimation. Moreover, the manipulator's cost takes into consideration the required batteries and extra materials for the joining.

The average price of cleaning 10 solar panels is 250 € and the required equipment is around 500 € [68]. The proposed implementation, in contrast, costs 16,556.90 €, which is up to twenty times the cost of the actual method. Being the quadrotor the 80% of the total budget, the selection of a cheaper UAV or the design of a new one could reduce the price to a more competitive value. The development of a specific quadrotor would be ideal since it could also expand the manipulator's range of action by increasing the limit angles. To do so, a retractable landing gear, for instance, could be of great help. Nevertheless, the expenses of such elaboration are uncertain.

Although the proposal's budget will still be higher, the fact that the UAV is a one-time purchase cannot be neglected. While manual cleaning is paid for on a regular basis, the drone implementation will only need changing the microfiber cloth and batteries. In fact, the former could be cleaned up once the UAV ends its journey, and then attached again to the mop for future uses.

Chapter 10

Conclusions and Future prospects

The main objective of the study was to develop a new implementation for cleaning solar panels using an UAV. Although there are few, some drones are already employed for this task. Nevertheless, in this project, an innovative proposal was made by adding a robotic manipulator, which has a microfiber cloth-coated mop attached. While the selection of the mop was extracted from an already-developed experimental study, using the manipulator for the cleaning task is the author's new contribution to this kind of study.

After researching the main features of the possible UAVs that can be implemented, the quadrotor was selected as the most suitable one. In fact, with an estimation of the payload, *Matrice 300 RTK* was found to be the best model with a maximum height from 5000 *to* 7000 m, and autonomy of 42 min when the payload is being carried. Unfortunately, the addition of the payload leads to the impossibility of using one of the autonomous positioning systems of the quadrotor. It should be noted that some of the main parameters of the UAV were not detailed, hence, values from literature are taken or computations from the accessible measurements are made.

Moreover, the initial proposal was that the drone could autonomously do the cleaning, but the authorities may disapprove the scenario due to its level of hazard. A more realistic approach would be using a pilot who should be careful with both, the people around and the possible interferences between the UAV and the pilot control.

Once the general overview of the prototype is selected, the proper design of the payload is done. Three different pieces are developed through *SOLIDWORKS*, a joining piece between the quadrotor and the manipulator, the manipulator itself, and the mop. The joining piece blueprint is achieved considering the joining piece for the payload the quadrotor has. The manipulator's length is set to 0.32 m due to the drone's landing gear influence. Finally, the mop is sized taking into account not only its weight but also its size in relation to the typical rooftop solar panels.

Developing the mathematical modeling of the quadrotor with the manipulator was a challenge due to the lack of accessible documents with the mathematical development. Despite the fact that the initial idea was to consider the quadrotor and the manipulator as one model, they are finally modeled separately with their

respective interference with the aim of easing the computations.

When it comes to the prototype's control, a new control strategy combining LQG controller for the quadrotor and PID controller for the arm, has been proposed and applied. A relatively stable control is accomplished through the adequate selection of the PID constants and the LQG design matrices.

Although *Matrice 300 RTK*'s LiPo batteries are prejudicial for the environment, the global environmental impact is positive. The proposal's implementation will not only cut off the water wasted but also help boost in renewable sources. Regarding the economic feasibility of the project, it is concluded that the drone selected is too expensive for the purpose. The existing methods are more economical and the implementation will not succeed.

As future work, a new UAV could be specially designed for the purpose. One of its main features should be a retractable landing gear, thus, the length and weight of the manipulator are reduced. Furthermore, experiments carried out to determine when the cloth should be removed due to efficiency loss could be done. Moreover, another cleaning method, the ECS for instance, could be implemented in the recharging station so as to clean the cloth. In addition, new control algorithms, such as adaptive control, could be developed for a better response.

Bibliography

1. *Solar energy* [online]. European Comission [visited on 2023-02]. Available from URL: https://energy.ec.europa.eu/topics/renewable-energy/solar-energy_en.
2. FROST, Rosie. *EU solar power soars by almost 50€ in 2022: Which country installed the most* [online]. Euronews, 2022 [visited on 2023-02]. Available from URL: https://www.euronews.com/green/2022/12/20/eu-solar-power-soars-by-almost-50-in-2022-which-country-installed-the-most.
3. LIMB, Lottie. *Live in an apartment? This new solar technology cut could your bills in half* [online]. Euronews, 2023 [visited on 2023-02]. Available from URL: https://www.euronews.com/green/2023/02/18/live-in-an-apartment-this-new-solar-technology-cut-could-your-bills-in-half.
4. SARAVANAN, V.S.; DARVEKAR, S.K. Solar Photovoltaic Panels Cleaning Methods A Review [online]. *International Journal of Pure and Applied Mathematics* [online]. 2018, vol. 118, no. 24 [visited on 2023-02]. Available from URL: http://www.acadpubl.eu/hub/.
5. BONAN, Edan. *How do you keep thousands of solar panels clean? Use a drone* [online]. No camels, 2022 [visited on 2023-02]. Available from URL: https://nocamels.com/2022/07/how-do-you-keep-thousands-of-solar-panels-clean-use-a-drone/.
6. *Cleandrone* [online]. Cleandrone [visited on 2023-02]. Available from URL: http://www.cleandrone.com/.
7. *Aerial roof and surface cleaning with spray UAV* [online]. DRONE VOLT, 2023 [visited on 2023-02]. Available from URL: https://www.dronevolt.com/en/aerial-roof-and-surface-cleaning-with-spray-uav/.
8. *A future based on renewable energy.* [online]. European Environment Agency, 2022 [visited on 2023-02]. Available from URL: https://www.eea.europa.eu/signals/signals-2022/articles/a-future-based-on-renewable-energy.
9. ELLERBECK, Stefan. *Wind and solar power generated more electricity in the EU last year than gas did. Here's how.* [online]. World Economic Forum, 2023-01 [visited on 2023-02]. Available from URL: https://www.weforum.org/agenda/2023/01/renewable-energy-electricity-record-europe/.
10. JONES, Dave. *European Electricity Review* [online]. Ember, 2023-01 [visited on 2023-02]. Available from URL: https://ember-climate.org/insights/research/european-electricity-review-2023/#supporting-material.
11. AL-HOUSANI, Mohammed; BICER, Yusuf; KOÇ, Muammer. Experimental investigations on PV cleaning of large-scale solar power plants in desert climates: Comparison of cleaning techniques for

drone refrofitting. *Energy Conversion and Management* [online]. 2019, vol. 185, pp. 800–815 [visited on 2023-02]. ISSN 0196-8904. Available from DOI: 10.1016/j.enconman.2019.01.058.

12. DEB, Dipankar; BRAHMBHATT, Nisarg L. Review of yield increase of solar panels through soiling prevention, and a proposed water-free automated cleaning solution. *Renewable and Sustainable Energy Reviews* [online]. 2018, vol. 82, pp. 3306–3313 [visited on 2023-02]. ISSN 1364-0321. Available from DOI: 10.1016/j.rser.2017.10.014.
13. SAYYAH, Arash; HORENSTEIN, Mark N.; MAZUMDER, Malay K. Energy yield loss caused by dust deposition on photovoltaic panels. *Solar Energy* [online]. 2014, vol. 107, pp. 576–604 [visited on 2023-02]. ISSN 0038-092X. Available from DOI: 10.1016/j.solener.2014.05.030.
14. REHMAN, S.; MOHANDES, M. A.; HUSSEIN, A. E.; ALHEMS, L. M.; AL-SHAIKHI, A. Cleaning of Photovoltaic Panels Utilizing the Downward Thrust of a Drone. *Energies 2022* [online]. 2022, vol. 15, no. 8159 [visited on 2023-02]. ISSN 1996-1073. Available from DOI: 10.3390/en15218159.
15. GRANDO, Marcel; MALETZ, Elias; MARTINS, Daniel; SIMAS, Henrique; SIMONI, Roberto. *Robots for Cleaning Photovoltaic Panels: State of the Art and Future Prospects* [online]. 2017-11. [visited on 2023-02]. Available from URL: %5Curl%7Bhttps://www.researchgate.net/publication/321831728_Robots_for_Cleaning_Photovoltaic_Panels_State_of_the_Art_and_Future_Prospects%7D.
16. FARROKHI DERAKHSHANDEH, Javad; ALLUQMAN, Rand; MOHAMMAD, Shahad; ALHUSSAIN, Haya; ALHENDI, Ghanima; ALEID, Dalal; AHMAD, Zainab. A comprehensive review of automatic cleaning system of solar panels. *Sustainable Energy Technologies and Assessments* [online]. 2021, vol. 47, p. 101518 [visited on 2023-02]. ISSN 2213-1388. Available from DOI: 10.1016/j.seta.2021.101518.
17. KAZEM, HHussein A.; CHAICHAN, Miqdam T.; AL-WAELI, Ali H.A.; SOPIAN, K. A review of dust accumulation and cleaning methods for solar photovoltaic systems. *Journal of Cleaner Production* [online]. 2020, vol. 276, p. 123187 [visited on 2023-02]. ISSN 0959-6526. Available from DOI: 10.1016/j.jclepro.2020.123187.
18. AKYAZI, Ömür; ŞAHIN, Erdinç; ÖZSOY, Timur; ALGÜL, Mehmet. A Solar Panel Cleaning Robot Design and Application. *Europea Journal of Science and Technology* [online]. 2019, pp. 343–348 [visited on 2023-02]. ISSN 2148-2683. Available from DOI: 10.31590/ejosat.638291.
19. KHALID, Haris M.; RAFIQUE, Zimran; MUYEEN, S.M.; RAQEEB, Abdul; SAID, Zafar; SAIDUR, R.; SOPIAN, Kamaruzzaman. Dust accumulation and aggregation on PV panels: An integrated survey on impacts, mathematical models, cleaning mechanisms, and possible sustainable solution. *Solar Energy* [online]. 2023, vol. 251, pp. 261–285 [visited on 2023-02]. ISSN 0038-092X. Available from DOI: 10.1016/j.solener.2023.01.010.
20. ALMALKI, Faris A.; ALBRAIKAN, Amani A.; SOUFIENE, Ben Othman; ALI, Obaid. Utilizing Artificial Intelligence and Lotus Effect in an Emerging Intelligent Drone for Perserving Solar Panel Efficiency. *Wireless Communications and Mobile Computing* [online]. 2022 [visited on 2023-02]. ISSN 1530-8669. Available from DOI: 10.1155/2022/7741535.
21. ALGHAMDI, Yousef; MUNIR, Arslan; LA, Hung Manh. Architecture, Classification, and Applications of Contemporary Unmanned Aerial Vehicles. *IEE Consumer Technology Society* [online]. 2021, vol. 10, no. 6, pp. 9–20 [visited on 2023-02]. Available from DOI: 10.1109/MCE.2021.3063945.

22. SINGHAL, Gaurav; BANSOD, Babankumar; MATHEW, Lini. Unmanned Aerial Vehicle Classification, Applications and Challenges: A Review [online]. 2018 [visited on 2023-02]. Available from DOI: 10.20944/preprints201811.0601.v1.
23. BOUDABDALLAH, Samir. Design and control of quadrotors with application to autonomous flying. *Lausanne, EPFL* [online]. 2007, p. 155 [visited on 2023-03]. Available from DOI: 10.5075/epfl-thesis-3727.
24. KIM, Suseong; CHOI, Seungwon; KIM, H. Jin. Aerial manipulation using a quadrotor with a two DOF robotic arm. In: *2013 IEEE/RSJ International Conference on Intelligent Robots and Systems* [online]. 2013, pp. 4990–4995 [visited on 2023-05]. Available from DOI: 10.1109/IROS.2013.6697077.
25. RUGGIERO, F.; TRUJILLO, M.A.; CANO, R.; ASCORBE, H.; VIGURIA, A.; PERÉZ, C.; LIPPIELLO, V.; OLLERO, A.; SICILIANO, B. A multilayer control for multirotor UAVs equipped with a servo robot arm. In: *2015 IEEE International Conference on Robotics and Automation (ICRA)* [online]. 2015, pp. 4014–4020 [visited on 2023-05]. Available from DOI: 10.1109/ICRA.2015.7139760.
26. GIGLIO, Gerardo; PIERRI, Francesco. Selective compliance control for an unmanned aerial vehicle with a robotic arm. In: *22nd Mediterranean Conference on Control and Automation* [online]. 2014, pp. 1190–1195 [visited on 2023-05]. Available from DOI: 10.1109/MED.2014.6961537.
27. JIAO, Ran; CHOU, Wusheng; DING, Rui; DONG, Mingjie. Adaptive robust control of quadrotor with a 2-degree-of-freedom robotic arm. *Advances in Mechanical Engineering* [online]. 2018, vol. 10, no. 8 [visited on 2023-05]. Available from DOI: 10.1177/1687814018778639.
28. *Bastidor Metalico Mopa 100cm* [online]. Hiperlimpieza, 2023 [visited on 2023-03]. Available from URL: https://www.ventadeproductosdelimpieza.es/bastidor-metalico-mopa-100-cm.
29. *Scotch-Brite. Bayeta Microfibra de alto rendimiento 2010* [online]. 3M España, 2023 [visited on 2023-03]. Available from URL: https://www.3m.com.es/3M/es_ES/p/d/b00038441/.
30. *Freefly Systems* [online]. Freefly [visited on 2023-04]. Available from URL: https://freeflysystems.com.
31. *Enterprise-DJI* [online]. DJI Official [visited on 2023-04]. Available from URL: https://www.dji.com/es/products/enterprise?site=enterprise&from=nav.
32. *DJI Inspire 2* [online]. Deltoc [visited on 2023-04]. Available from URL: https://www.deltoc.com/producto/dji-inspire-2.
33. *Draganflyer Commander 2* [online]. Draganfly [visited on 2023-04]. Available from URL: https://draganfly.com/draganflyer-commander2/.
34. *Parrot ANAFI Ai- The 4G robotic UAV* [online]. Parrot [visited on 2023-04]. Available from URL: https://www.parrot.com/us/drones/anafi-ai.
35. *Skydio 2+ Enterprise Drone* [online]. Skydio Inc [visited on 2023-04]. Available from URL: https://www.skydio.com/skydio-2-plus-enterprise.
36. FRED. *Industria, ejército: se acercan los Skydio X2E y X2D* [online]. Helicomicro, 2020-07 [visited on 2023-04]. Available from URL: https://www.helicomicro.com/2020/07/13/industrie-armee-les-skydio-x2e-et-x2d-sont-en-approche/.

37. *Matrice 300 RTK. User Manual v1.0* [online]. DJI, 2020 [visited on 2023-05]. Available from URL: https://enterprise.dji.com/es/matrice-300/downloads.
38. *What is RTK and what does it stand for?* [online]. Global GPS Systems [visited on 2023-05]. Available from URL: https://globalgpssystems.com/gnss/what-is-rtk-and-what-does-it-stand-for/.
39. *Matrice 300 RTK Redundant Systems Report* [online]. DJI, 2020 [visited on 2023-05]. Available from URL: https://terra-1-g.djicdn.com/851d20f7b9f64838a34cd02351370894/Matrice_300RTK_Redundant_Systems_Report.pdf.
40. *IP ratings* [online]. IEC [visited on 2023-05]. Available from URL: https://www.iec.ch/ip-ratings.
41. *Matrice 300 RTK 3D Model* [online]. DJI, 2021 [visited on 2023-05]. Available from URL: https://enterprise.dji.com/es/matrice-300/downloads.
42. SANCA, Armando S.; ALSINA, Pablo J.; CERQUEIRA, Jés de Jesus F. Dynamic Modelling of a Quadrotor Aerial Vehicle with Nonlinear Inputs. In: *2008 IEEE Latin American Robotic Symposium* [online]. 2008, pp. 143–148 [visited on 2023-05]. Available from DOI: 10.1109/LARS.2008.17.
43. *Easy Access Rules for Unmanned Aircraft Systems (Regulations (EU) 2019/947 and 2019/945)* [online]. EASA, 2022-09 [visited on 2023-03].
44. *Civil drones (unmanned aircraft)* [online]. EASA, 2023-06 [visited on 2023-03]. Available from URL: https://www.easa.europa.eu/en/domains/civil-drones.
45. *Formación de pilotos UAS/drones en categoría 'abierta'* [online]. AESA-Agencia Estatal de Seguridad Aérea-Ministerio de Fomento. [visited on 2023-04]. Available from URL: https://www.seguridadaerea.gob.es/es/ambitos/drones/formacion-de-pilotos-a-distancia-de-uas-drones/formacion-de-pilotos-uas-drones-en-categoria-rabiertar.
46. *Solar Panel Dimension* [online]. Airis Solutions [visited on 2023-03]. Available from URL: https://airisenergy.us/solar-panels-dimensions/.
47. *Power HD Servo Estándar de Alto Torque HD-1501MG* [online]. SanDoRobotics [visited on 2023-05]. Available from URL: https://sandorobotics.com/producto/hd-1501mg/.
48. FERNANDO, H. C. T. E.; DE SILVA, A. T. A.; DE ZOYSA, M. D. C.; DILSHAN, K. A. D. C.; MUNASINGHE, S. R. Modelling, Simulation and Implementation of a Quadrotor UAV [online]. 2013, pp. 207–212 [visited on 2023-04]. Available from DOI: 10.1109/ICIInfS.2013.6731982.
49. FENG, Ying; RABBATH, Camille Alain; SU, Chun-Yi". Modelling of a Micro UAV with Slung Payload [online]. 2015, pp. 1257–1272 [visited on 2023-04]. Available from DOI: 10.1007/978-90-481-9707-1_108.
50. LU, Qi; REN, Beibei; PARAMESWARAN, Siva; ZHONG, Qing-Chang. Uncertainty and Disturbance Estimator-Based Robust Trajectory Tracking Control for a Quadrotor in a GPS-denied Environment. *Journal of Dynamic Systems, Measurement, and Control* [online]. 2017, vol. 140 [visited on 2023-06]. Available from DOI: 10.1115/1.4037736.
51. SELBY, Wil. *Quadrotor System Modelling* [online]. 2015-05. [visited on 2023-03]. Available from URL: https://wilselby.com/research/arducopter/modeling/.

52. JZYL. *Answer to: "The relation between Euler-angle rate and body-axis rates?"* [online]. Aviation Stack Exchange, 2021-03 [visited on 2023-03]. Available from URL: `https://aviation.stackexchange.com/a/84008`.

53. ZHANG, Xiaodong; LI, Xiaoli; WANG, Kang; L, Yanjun. A Survey of Modelling and Identification of a Quadrotor Robot [online]. 2014 [visited on 2023-04]. Available from DOI: `10.1155/2014/320526`.

54. HORYNAD, Jiri. *Robotic manipulation onboard an unmanned aerial vehicle* [online]. Bachelor's Thesis, Faculty of Electrical Engineering, CZECH TECHNICAL UNIVERSITY IN PRAGUE, Department of Cybernetics, 2018 [visited on 2023-05].

55. BAZYLEV, Dmitry; KREMLEV, Artem; MARGUN, Alexey; ZIMENKO, Konstantin. Design of control system for a four-rotor UAV equipped with robotic arm. In: *2015 7th International Congress on Ultra Modern Telecommunications and Control Systems and Workshops (ICUMT)*. 2015, pp. 144–149. Available from DOI: `10.1109/ICUMT.2015.7382419`.

56. TEDRAKE, Russ. *Underactuacted Robotics*. Ch22-Multibody Dynamics [online]. 2023. [visited on 2023-03]. Available from URL: `https://shorturl.at/oyT39`.

57. KANNAN, Somasundar; ALMA, Marouane; OLIVARES-MENDEZ, Miguel; VOOS, Holger. Adaptive control of Aerial Manipulation Vehicle. *Proceedings - 4th IEEE International Conference on Control System, Computing and Engineering, ICCSCE 2014* [online]. 2015, pp. 273–278 [visited on 2023-06]. Available from DOI: `10.1109/ICCSCE.2014.7072729`.

58. CANO, Antonio Enrique Jiménez. Control de un quadrotor con un brazo manipulador. *Departamento de ingeniería de ingeniería de sistemas y automática. Universidad de Sevilla* [online]. 2012 [visited on 2023-06].

59. *Proportional Integral Derivative. Dynamics and Control* [online]. 2022. [visited on 2023-06]. Available from URL: `https://apmonitor.com/pdc/index.php/Main/ProportionalIntegralDerivative`.

60. MARTINS, Luís; CARDEIRA, Carlos; OLIVEIRA, Paulo. Linear Quadratic Regulator for Trajectory Tracking of a Quadrotor. *IFAC-PapersOnLine*. 2019, vol. 52, no. 12, pp. 176–181. ISSN 2405-8963. Available from DOI: `https://doi.org/10.1016/j.ifacol.2019.11.195`. 21st IFAC Symposium on Automatic Control in Aerospace ACA 2019.

61. PEÑA, Mauricio Vladimir; VIVAS, Edilberto Carlos; RODRÍGUEZ, Carol Ivonn. Simulation of the quadrotor controlled with LQR with integral effect. *ABCM Symposium Series in Mechatronics. Section II-Control Systems*. 2012, vol. 5, pp. 390–399. Available from URL: `https://abcm.org.br/symposium-series/SSM_Vol5/Section_II_Control_Systems/19321.pdf`.

62. WELCH, Greg; BISHOP, Gary. An Introduction to the Kalman Filter. *Proc. Siggraph Course* [online]. 2006, vol. 8 [visited on 2023-06].

63. ALI, Zain; LI, Xinde. Modeling and controlling of quadrotor aerial vehicle equipped with a gripper. *Measurement and Control* [online]. 2019, vol. 52, p. 002029401983404 [visited on 2023-06]. Available from DOI: `10.1177/0020294019834040`.

64. *Electric energy emission factor: the electric mix* [online]. 2022. [visited on 2023-06]. Available from URL: `https://canviclimatic.gencat.cat/en/actua/factors_demissio_associats_a_lenergia/`.

65. PETER. *What is the Environmental Impact of Lithium Batteries?* [online]. Cenex- Connected Automated Mobility [visited on 2023-06]. Available from URL: `https://www.cenex-lcv.co.uk/news-media/exhibitor/what-is-the-environmental-impact-of-lithium-batteries`.

66. *How Long Does LiPo Battery Last?* [online]. UniEnergy Technologies Battery [visited on 2023-06]. Available from URL: `https://www.uetechnologies.com/how-long-does-lipo-battery-last/#Whats_The_Lifespan_of_a_LiPo_Battery`.

67. *How much does a robotic arm cost?* [online]. HitBot [visited on 2023-06]. Available from URL: `https://www.hitbotrobot.com/a-robotic-arm-cost/`.

68. *Precios y Presupuestos para el Mantenimiento de Placas Solares* [online]. habitissimo, 2022 [visited on 2023-06]. Available from URL: `https://www.habitissimo.es/presupuestos/hacer-mantenimiento-placas-solares`.